D-*myo*-Inositol-3-Phosphate Affects Phosphatidylinositol-Mediated Endomembrane Function in *Arabidopsis* and Is Essential for Auxin-Regulated Embryogenesis [W][OA]

Yu Luo,[a] Genji Qin,[a] Jun Zhang,[a] Yuan Liang,[b] Yingqi Song,[a] Meiping Zhao,[b] Tomohiko Tsuge,[c] Takashi Aoyama,[c] Jingjing Liu,[a] Hongya Gu,[a,d] and Li-Jia Qu[a,d,1]

[a] State Key Laboratory of Protein and Plant Gene Research, College of Life Sciences, Peking University, Beijing 100871, People's Republic of China
[b] College of Chemistry and Molecular Engineering, Peking University, Beijing 100871, People's Republic of China
[c] Institute for Chemical Research, Kyoto University, Gokasho Uji, Kyoto 611-0011, Japan
[d] The National Plant Gene Research Center (Beijing), Beijing 100101, People's Republic of China

In animal cells, *myo*-inositol is an important regulatory molecule in several physiological and biochemical processes, including signal transduction and membrane biogenesis. However, the fundamental biological functions of *myo*-inositol are still far from clear in plants. Here, we report the genetic characterization of three *Arabidopsis thaliana* genes encoding D-*myo*-inositol-3-phosphate synthase (MIPS), which catalyzes the rate-limiting step in de novo synthesis of *myo*-inositol. Each of the three *MIPS* genes rescued the yeast *ino1* mutant, which is defective in yeast MIPS gene *INO1*, and they had different dynamic expression patterns during *Arabidopsis* embryo development. Although single *mips* mutants showed no obvious phenotypes, the *mips1 mips2* double mutant and the *mips1 mips2 mips3* triple mutant were embryo lethal, whereas the *mips1 mips3* and *mips1 mips2*^{+/−} double mutants had abnormal embryos. The *mips* phenotypes resembled those of auxin mutants. Indeed, the double and triple *mips* mutants displayed abnormal expression patterns of DR5:green fluorescent protein, an auxin-responsive fusion protein, and they had altered PIN1 subcellular localization. Also, membrane trafficking was affected in *mips1 mips3*. Interestingly, overexpression of *PHOSPHATIDYLINOSITOL SYNTHASE2*, which converts *myo*-inositol to membrane phosphatidylinositol (PtdIns), largely rescued the cotyledon and endomembrane defects in *mips1 mips3*. We conclude that *myo*-inositol serves as the main substrate for synthesizing PtdIns and phosphatidylinositides, which are essential for endomembrane structure and trafficking and thus for auxin-regulated embryogenesis.

INTRODUCTION

myo-inositol is the most important and abundant stereoisomer of the six-carbon cyclitol inositol. It exists in all eukaryotes and is also found in some prokaryotes (Eagle et al., 1957; Bachhawat and Mande, 2000). *myo*-inositol emerged early during evolution and evolved into diverse derivatives, such as phosphoinositides (PIs), inositol phosphates, glycosylphosphatidylinositol, and various inositol conjugates (Michell, 2008). Inositol and its derivatives are involved in various biochemical and physiological processes, including intracellular signal transduction (Irvine and Schell, 2001), membrane construction and trafficking (Cullen et al., 2001), membrane-related protein anchoring (Tiede et al., 1999; Peskan et al., 2000; Borner et al., 2005), and cell wall construction (Loewus 1973). They also act as protein cofactors (Macbeth et al., 2005; Tan et al., 2007) and play roles in auxin storage and trafficking in plant seeds (Hall and Bandurski, 1986).

In mammalian cells, *myo*-inositol and its derivatives play important roles in reproduction (Chiu et al., 2003; Papaleo et al., 2009), embryo development (Kane et al., 1992; Greene and Copp, 1997; Hynes et al., 2000), and neuron function (Hanley et al., 1988; Fisher et al., 2002). Disruption of inositol homeostasis is reported to be a factor in bipolar disorder (Shaltiel et al., 2004) and neurodegenerative diseases, including Alzheimer's disease (Miller et al., 1993), Huntington's disease, and Parkinson's disease (Sarkar et al., 2005). Recently, inositol deficiency was shown to induce a neonatally lethal phenotype in mice (Buccafusca et al., 2008).

The cellular *myo*-inositol pool in mammalian cells is maintained by a combination of de novo biosynthesis, uptake from intracellular matrix, and recycling from PIs. D-*MYO*-INOSITOL-3-PHOSPHATE SYNTHASE (MIPS) has the most important role in de novo synthesis of inositol by catalyzing the rate-limiting step using glucose-6-phosphate as the substrate. MIPS is highly conserved among eukaryotes (Loewus and Murthy, 2000; Majumder et al., 2003). The first gene encoding MIPS to be identified was yeast *INO1* (Culbertson et al., 1976; Donahue and Henry, 1981). Since then, many *MIPS* genes have been identified in various prokaryotic and eukaryotic cells. In plants, characterization of

MIPSs from diverse plant species revealed their important roles in stress responses (Nelson et al., 1998; Ghosh Dastidar et al., 2006; Murphy et al., 2008) and in the regulation of phytate, the fully phosphorylated form of *myo*-inositol and the major phosphorus storage compound in seeds (Hegeman et al., 2001; Brinch-Pedersen et al., 2002; Stevenson-Paulik et al., 2005). There are three *MIPS* genes in *Arabidopsis*; the *MIPS1* gene was the first to be functionally identified by complementation of the yeast *ino1* mutant and to date is the best-characterized *MIPS* gene (Johnson and Sussex, 1995). Recently, a loss-of-function *MIPS1* mutant, *mips1*, was reported to exhibit impaired pathogen resistance (Murphy et al., 2008), programmed cell death (PCD) in leaves (Meng et al., 2009; Donahue et al., 2010), and deformed cotyledon development (Chen and Xiong, 2010).

Once synthesized, *myo*-inositol acts as a substrate for the formation of various inositol-derived molecules, for instance, phosphatidylinositol (PtdIns) and indole-3-acetic acid (IAA)-*myo*-inositol conjugates. PtdIns contribute 21% of the phospholipids in nonphotosynthetic plant membranes (Harwood, 1980), and the various phosphorylated forms of PtdIns, known as PIs, have critical roles in cytoskeletal rearrangements, membrane trafficking, and organelle labeling (Simonsen et al., 2001; Cantley, 2002; Thole and Nielsen, 2008). In mammalian systems, $Ins(1,4,5)P_3$, the hydrolyzed product of $PtdIns(4,5)P_2$, plays important roles in intracellular signal transduction as a second messenger. To date, however, there is no direct proof that $Ins(1,4,5)P_3$-mediated signaling exists in plants (Wheeler and Brownlee, 2008). The *Arabidopsis thaliana PHOSPHATIDYLINOSITOL SYNTHASE1* (*PIS1*) gene (At1g68000) and *PIS2* gene (At4g38570) are responsible for the net synthesis of PtdIns from *myo*-inositol and cytidine 5′-diphospho-1,2-diacyl-sn-glycerol (CDP-diacylglycerol) (Collin et al., 1999; Xue et al., 2000). As demonstrated in maize (*Zea mays*), *myo*-inositol can also form an IAA-*myo*-inositol conjugate (Normanly, 2010), the reaction of which involves two steps (Kesy and Bandurski, 1990). The first and rate-limiting step of this reaction, which is reversible, is specifically catalyzed by UDP-*GLUCOSYL TRANSFERASE* 84B1, encoded by *UGT84B1* (At2g23260) in *Arabidopsis* (Jackson et al., 2001). For the second step in maize, IAA moiety was transacylated from IAA-glucose to *myo*-inositol with a large negative free energy change (Kesy and Bandurski, 1990). However, no corresponding gene responsible for the second step has yet been found in *Arabidopsis*. Therefore, it remains to be investigated whether IAA-*myo*-inositol conjugates are present in *Arabidopsis*.

Plant *MIPS* genes are highly expressed in developing seeds (Johnson and Wang, 1996; Yoshida et al., 1999; Hegeman et al., 2001; Abreu and Aragão, 2007; Mitsuhashi et al., 2008), suggesting that *myo*-inositol has an important role in seed/embryo development. In this study, we used genetic approaches to investigate the roles of three *MIPS* genes in *Arabidopsis* development, especially in embryo development. Of the three genes, *MIPS1* showed the most comprehensive and long-lasting expression during seed development. For each of the *MIPS* genes, single null mutants showed no visible phenotypes, but the double mutants *mips1 mips2*^{+/−} and *mips1 mips3* displayed severe defects in embryogenesis, producing altered numbers of cotyledons (one to four) with deformed shapes. Furthermore, the homozygous *mips1 mips2* and *mips1 mips2 mips3* triple mutants

were embryonic lethal, suggesting that de novo synthesis of *myo*-inositol is critical. Our data suggest that the developmental defects of *mips* mutants are caused by altered auxin transport and responses in the double and triple mutants. Interestingly, overexpression of *PIS2* largely rescued the abnormal embryo phenotypes in the *mips1 mips3* double mutant, restoring the shape and number of cotyledons, and also the endomembrane function, whereas overexpression of *UGT84B1* enhanced the cotyledon phenotypes. The fact that *PIS2* largely rescued the *myo*-inositol deficiency phenotype suggests that the defects in *mips1 mips3* resulted from decreased levels of membrane PtdIns. We conclude that MIPS-mediated de novo synthesis of *myo*-inositol is essential for maintaining the normal function of endomembrane trafficking and for maintaining endomembrane structure, which is critical for the correct auxin transport and, thus, correct auxin localization during embryo pattern formation.

RESULTS

Arabidopsis MIPS Genes Rescued the Yeast Inositol Auxotrophy Mutant *ino1*

As a highly conserved enzyme, MIPS is found in all eukaryotes and a few prokaryotes. In the phylogenetic tree constructed with more than 100 eukaryotic MIPS protein sequences using PHYLIP (Felsenstein, 2005), MIPSs from plants form an independent subgroup (see Supplemental Figure 1 online), and multiple copies of the *MIPS* gene emerge only in land plant species. There are three putative *MIPS* homologous genes in the *Arabidopsis* genome. It appears that *MIPS3* diverted from the ancestor of *MIPS1* and *MIPS2* at an early stage of evolution as the result of duplication and then a recent duplication event produced *MIPS1* and *MIPS2*. We first investigated whether all three genes are functional. The yeast *myo*-inositol auxotrophy mutant *ino1* cannot survive in the absence of *myo*-inositol because of a deletion in the *INO1* gene (Nunez et al., 2008). We generated constructs containing each of the *Arabidopsis MIPS* genes driven by a constitutive *GPD* promoter and transformed them into the yeast mutant *ino1*, with empty vector–transformed *ino1* as the negative control and yeast innate *INO1*-transformed *ino1* as the positive control. The yeast *INO1* gene rescued the *ino1* mutant as expected (Figure 1). The three *Arabidopsis MIPS* genes also rescued the yeast *ino1* mutant (Figure 1). This result showed that each of the three *MIPS* genes is a functional counterpart of yeast *INO1* in *Arabidopsis*, furthermore showing that the inositol biosynthetic pathways are highly conserved between yeast and plants. Since the three *Arabidopsis* MIPSs shared ∼90% identity at the amino acid level and were all able to rescue yeast *ino1* mutant, the evolution of these *MIPS* genes possibly represents diversification of temporal and spatial regulation rather than changes in amino acid sequences or catalytic capacity.

The Three *MIPS* Genes Showed Different Expression Patterns and Levels during Embryogenesis

We first used quantitative RT-PCR to examine the transcript levels of each of the *MIPS* genes in different *Arabidopsis* tissues
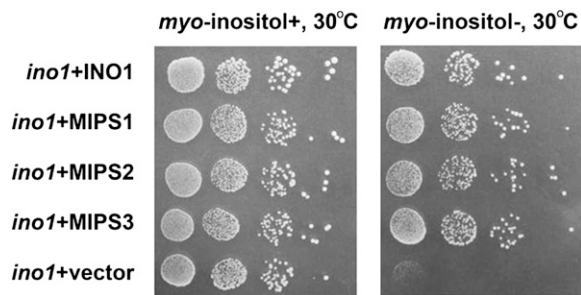
Figure 1. Complementation of the Yeast *ino1* Mutant.

Expression of each of the three *Arabidopsis MIPS* complements the inositol auxotrophy phenotype of the yeast *ino1* mutant. The yeast cells transformed with *INO1* or empty vector were used as positive and negative controls, respectively. Plates were spotted with 10-fold serial dilutions and incubated at 30°C for 2 d.

and organs. All of the *MIPS* genes were expressed in the tested tissues (Figure 2; see Supplemental Figure 2 online), consistent with a previous report (Donahue et al., 2010). The highest expression levels of *MIPS1* were observed in siliques (Figure 2), which is consistent with results from microarray analyses (Zimmermann et al., 2004).

To analyze the expression patterns in more detail, we generated constructs with 2-kb promoter fragments of each of the *MIPS* genes driving the *uidA* reporter gene and introduced these constructs into *Arabidopsis*. The overall β-glucuronidase (GUS) staining patterns in siliques differed among the three *MIPS* genes (i.e., *MIPS1* was specifically expressed in developing seeds, *MIPS2* was highly expressed in the seedpods and seeds, and *MIPS3* was expressed in the funiculi and vascular tissues of seedpods) (Figures 3A to 3C). *MIPS1* expression was detectable throughout embryo development, from the early globular stage to the mature stage in both the embryo and the endosperm (Figures 3D to 3G), but not in the seed coat from the torpedo (Figure 3F) to the mature stages (Figure 3G). At the globular stage, the expression patterns of *MIPS2* and *MIPS3* were similar to that of *MIPS1* (Figures 3H and 3L). However, unlike *MIPS1*, *MIPS2* and *MIPS3* were not expressed in embryos after the globular stage. We detected some *MIPS2* signals in seed coats at the heart stage (Figure 3I) and in endosperm at the torpedo stage (Figure 3J). At the heart and torpedo stages, *MIPS3* was expressed only in the funiculi (Figures 3M and 3N). *MIPS2* and *MIPS3* were not expressed in mature seeds (Figures 3K and 3O). The results suggest that the transcription of the three *MIPS* genes is coordinately regulated during seed development and that they might function differently in different tissues.

Single *mips* Mutants Showed No Obvious Phenotypes during Embryo and Leaf Development

To examine the biological roles of the three *MIPS* genes, we obtained the T-DNA insertion lines for *MIPS1* (SALK_023626) and *MIPS2* (SALK_031685) from the ABRC and identified a T-DNA insertion line of *MIPS3* from the mutant collection generated in our own laboratory (Qin et al., 2005). The insertion sites

of the three single mutants were all confirmed by sequencing (Figure 4A). RT-PCR analysis showed that no transcripts were detectable in the homozygous *mips1*, *mips2*, and *mips3* mutants (Figure 4B). We observed no abnormal phenotypes, including the embryo development, for three homozygous single mutants under optimal growth conditions (120 μmol m^{-2} s^{-1}, 16 h light/8 h dark) (Figure 4C). To further confirm that the single mutants of these three *MIPS* genes are normal, we analyzed more T-DNA insertion alleles of each *MIPS* gene (Figure 4A). No abnormal phenotypes were observed during embryogenesis under optimal growth conditions (Figure 4D). These results suggest that the three *MIPS* genes are probably functionally redundant.

Single *mips* Mutants Were Sensitive to High Light Intensity Stress

Although under the optimal growth condition no abnormal phenotype was observed for *mips1* (SALK_023626) in this study and another previous study (Murphy et al., 2008), this mutant was recently reported to be abnormal either during embryogenesis (i.e., affected cotyledon development) (Chen and Xiong, 2010; Donahue et al., 2010) or during postembryogenesis (i.e., induced lesion-mimic phenotypes in its rosette leaves under long-day conditions) (Meng et al., 2009; Donahue et al., 2010). To help clarify the phenotype discrepancy of *mips1* among different research groups, we grew the *mips1* single mutant plants under long-day conditions (16 h light/8 h dark) with different light intensities and examined embryogenesis and leaf development. We found that, while plants grown under lower light intensity showed no obvious phenotypes, plants grown under high light intensity (i.e., 160 μmol m^{-2} s^{-1} and 220 μmol m^{-2} s^{-1}) showed lesion-mimic phenotypes and that the higher light intensity
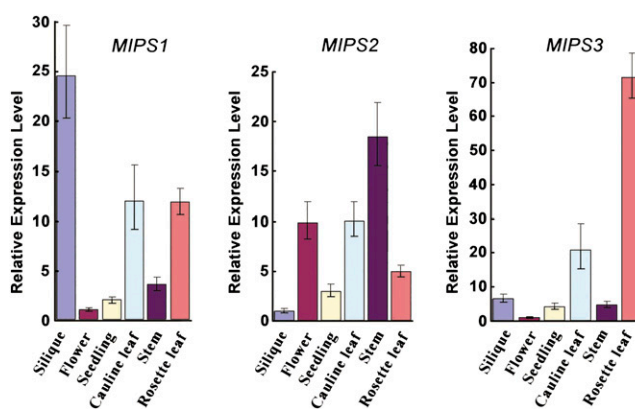

Figure 2. Relative Expression Level of *MIPS* Genes in Different *Arabidopsis* Tissues.

MIPS1, *MIPS1*, and *MIPS3* mRNA transcript levels in 8-DAG seedlings grown on half-strength Murashige and Skoog medium and in different organs of soil-grown *Arabidopsis* plants were quantified by real-time PCR. The expression levels for all genes were normalized to that of *TUB2*. Error bars were calculated as SE for three independent experiments.
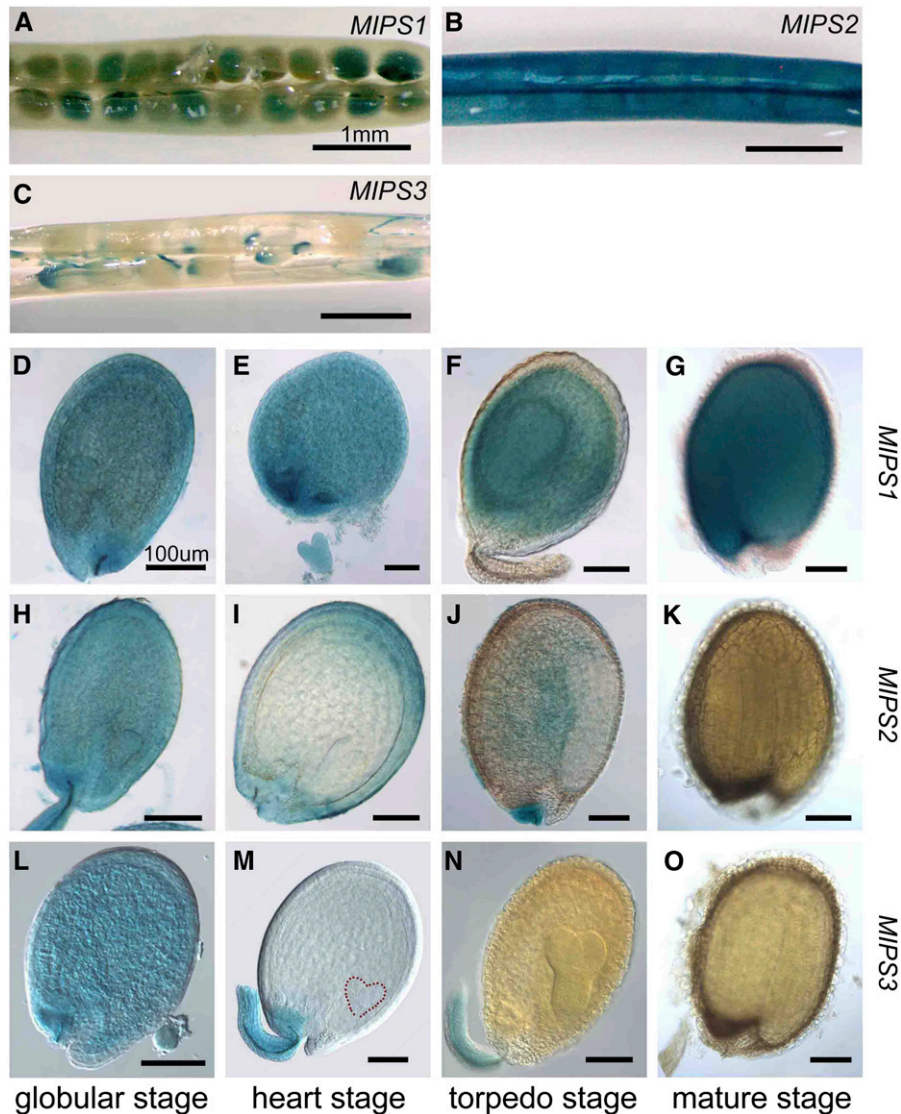
Figure 3. Dynamic Expression of *MIPS* Genes in Seed Development.

(A) to **(C)** GUS staining pattern of siliques from *MIPS1:GUS* **(A)**, *MIPS2:GUS* **(B)**, and *MIPS3:GUS* **(C)** transgenic lines. These seeds contain early torpedo stage embryos. Bars = 1 mm.

(D) to **(G)** GUS staining of seeds from *MIPS1:GUS* transgenic lines in sequential developmental stages as shown at the bottom of the figure. Bars = 100 μm.

(H) to **(K)** GUS staining of seeds from *pMIPS2:GUS* transgenic lines in sequential developmental stages. Bars = 100 μm.

(L) to **(O)** GUS staining of seeds from *pMIPS3:GUS* transgenic lines in sequential developmental stages. Bars = 100 μm.

applied the more severe lesion-mimic phenotypes developed (Figure 5A). To further investigate whether cotyledon development was affected, we examined cotyledon development in the seeds of *mips1* plants grown under different light intensity conditions. The results showed that, while displaying normal embryo and postembryo development under the 60 μmol m^{-2} s^{-1} or 120 μmol m^{-2} s^{-1} light conditions, *mips1* produced offspring with abnormal cotyledons under high light intensity conditions (i.e., 3.1% abnormal cotyledons under 160 μmol m^{-2} s^{-1} and 5.4% under 220 μmol m^{-2} s^{-1}) (Figure 5B). The severity of

mips1 phenotypes positively correlated to the light intensity (Figures 5A and 5B). These results suggest that loss of function of the major *MIPS* would lead to hypersensitivity of the plants to high light intensity stress. Together with the recent report that oxidative stress could greatly reduce the cellular *myo*-inositol level without affecting *MIPS1* function (Chaouch and Noctor, 2010), it seems that the phenotype discrepancy is possibly due to the different growth conditions applied (e.g., light intensity) and that the observed phenotypes are possibly attributed to the coaction of light intensity and partial loss of *MIPS* function.
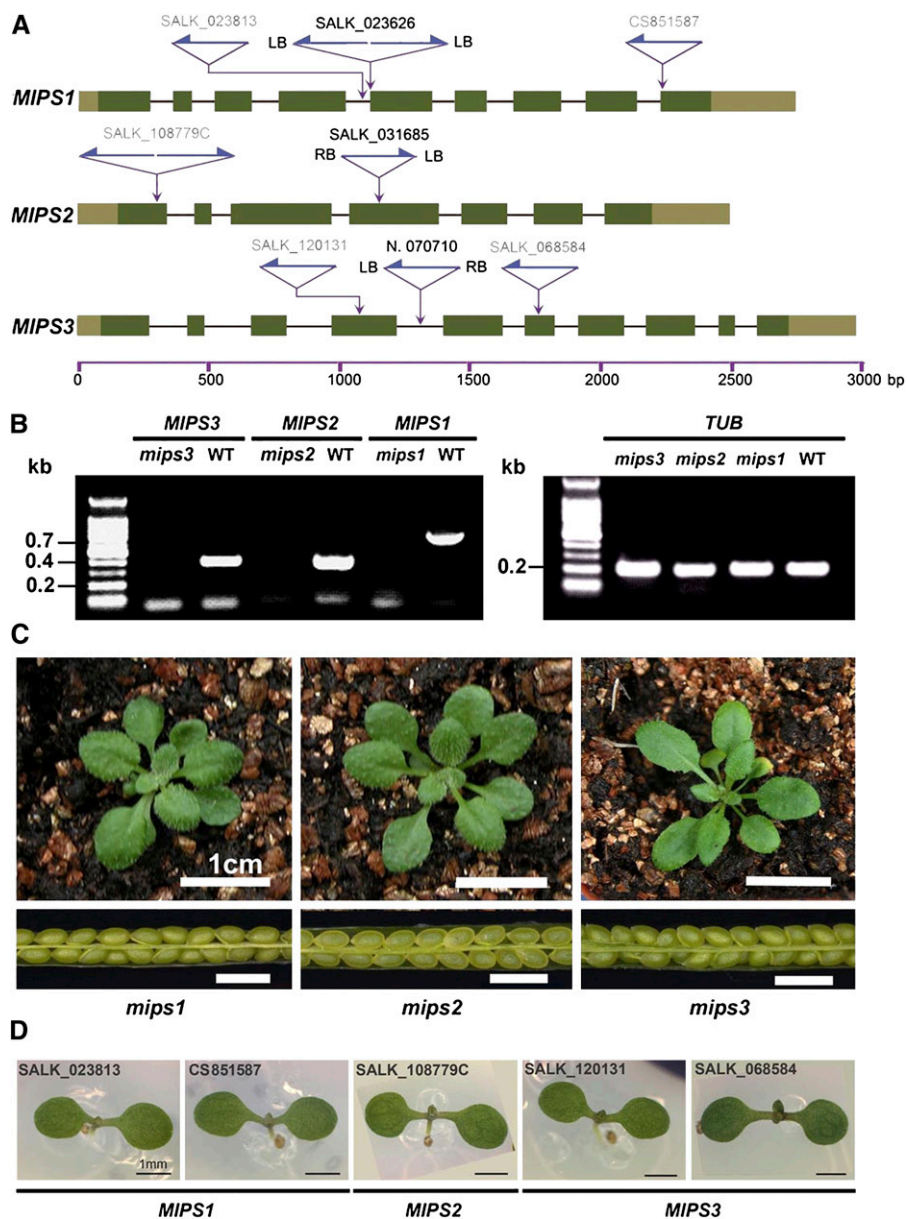
Figure 4. Expression and Phenotype Analysis of T-DNA Insertion Mutants for Each *MIPS* Gene.

(A) Gene structures of *MIPS1*, *MIPS2*, and *MIPS3* with the location of T-DNA insertions. The left border of each insertion was confirmed by sequencing. Exons (dark-green boxes indicate coding regions; lighter boxes indicate 5′ [left] and 3′ [right] untranslated regions) and T-DNA insertion sites (purple arrows) are indicated. SALK lines written in black are those used in further analysis and crossing. SALK lines written in gray are used in phenotype confirmation. LB, T-DNA left border; RB, T-DNA right border. Gene organizations are depicted in proportion.

(B) Transcript levels of *MIPS1*, *MIPS2*, *MIPS3* (left panel), and the internal control *TUB2* (right panel) in wild-type (WT) and three *mips* T-DNA insertion mutants were determined using RT-PCR (32 cycles).

(C) The 20-DAG seedling (top row) and seed (bottom row) phenotypes of *mips1* (left panels), *mips2* (middle panels), and *mips3* (right panels) single knockout mutants under the 16-h-light and 8-h-dark optimal growth condition. Bars = 1 cm.

(D) Normal cotyledon phenotype in different homozygous *mips* single mutants. T-DNA insertion lines for three *MIPS* genes were grown under the long-day light (120 μmol m^{-2} s^{-1}) optimal condition. The T-DNA insertion sites and the genotypes were confirmed by PCR. Bars = 1mm.
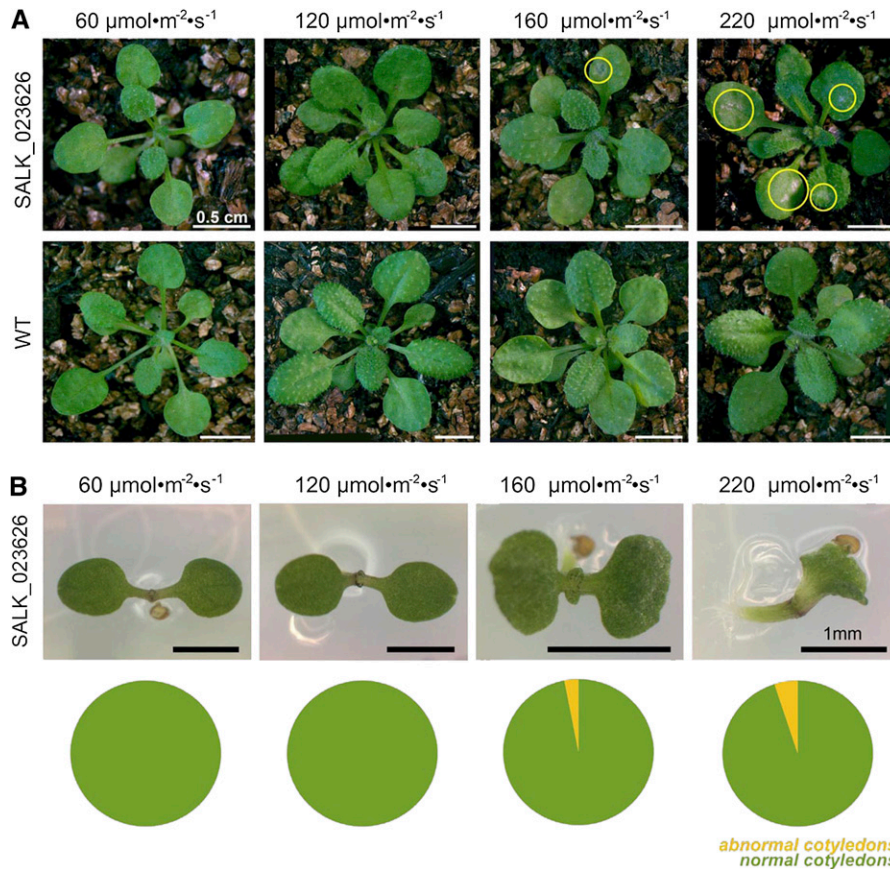
Figure 5. The Phenotypes of *mips1* under Different Light Intensity Conditions.

(A) Rosette leaf phenotypes of *mips1* (SALK_023626) grown under different light intensity conditions in comparison with the wild type (WT). Yellow circles indicate lesion-mimic patches. Bars = 0.5 cm.
(B) Cotyledon phenotypes of the seeds from *mips1* (SALK_023626) grown under different light intensity conditions. Each pie chart shows the percentage of the cotyledon phenotype proportion. Lime sectors represent the normal cotyledons and yellow sectors represent the abnormal cotyledons. Bars = 1 mm.

MIPS Mutant Combinations Produced Abnormal Cotyledons

To elucidate the physiological function of *MIPS* genes, we generated higher orders of *MIPS* mutants. Compared with the wild type (Figure 6A), the *mips1*$^{+/-}$ *mips2 mips3* triple mutant had no obvious phenotypes (see Supplemental Figure 3B online), possibly due to the higher expression level of *MIPS1* in the *mips2* mutant (Donahue et al., 2010), while *mips1 mips2*$^{+/-}$ displayed lesions in rosette and cauline leaves (see Supplemental Figure 3C online) under optimal growth condition (120 μmol m^{-2} s^{-1}, 16 h light/8 h dark). The *mips1 mips3* double mutant displays severe postembryonic phenotypes, including anthocyanidin accumulation in rosette leaves and much smaller adult plants compared with the wild type (see Supplemental Figure 3D online). In plants, anthocyanidin was reported to accumulate under stress conditions and to play important roles against UV irradiation and oxidative damage (Winkel-Shirley, 2002). The fact that the *mips1 mips3* mutants showed anthocyanidin accumulation under optimal growth conditions suggests that the depletion of *myo*-inositol causes constitutive stress response in *Arabidopsis*. Trypan blue staining results indicated programmed cell death in *mips1 mips2*$^{+/-}$ leaf lesions (see Supplemental Figure 3G online), while leaves from the wild type and *mips1 mips3* double mutant showed negative staining results (see Supplemental Figure 3H online).

It is interesting to notice that both *mips1 mips2*$^{+/-}$ (Figures 6B to 6D) and *mips1 mips3* (Figures 6E to 6G) double mutants had cotyledons that were fused at the basal end. In addition, the number of cotyledons in *mips1 mips3* was also altered, ranging from one to four, and approximately half of the two-cotyledon seedlings lacked bilateral symmetry (Table 1, Figures 6E to 6G). These cotyledon phenotypes of *mips1 mips3* were complemented by reintroduction of a *MIPS1* gene (Figure 6H). Symmetrical and asymmetrical cotyledons of both *mips1 mips2*$^{+/-}$ and *mips1 mips3* showed distorted vascular systems, such as parallel veins (Figure 6I), clustered bundles of irregular veins (Figure 6J), and discontinuous or poorly axialized venation patterns (Figure 6K). Scanning electron microscopy analysis revealed
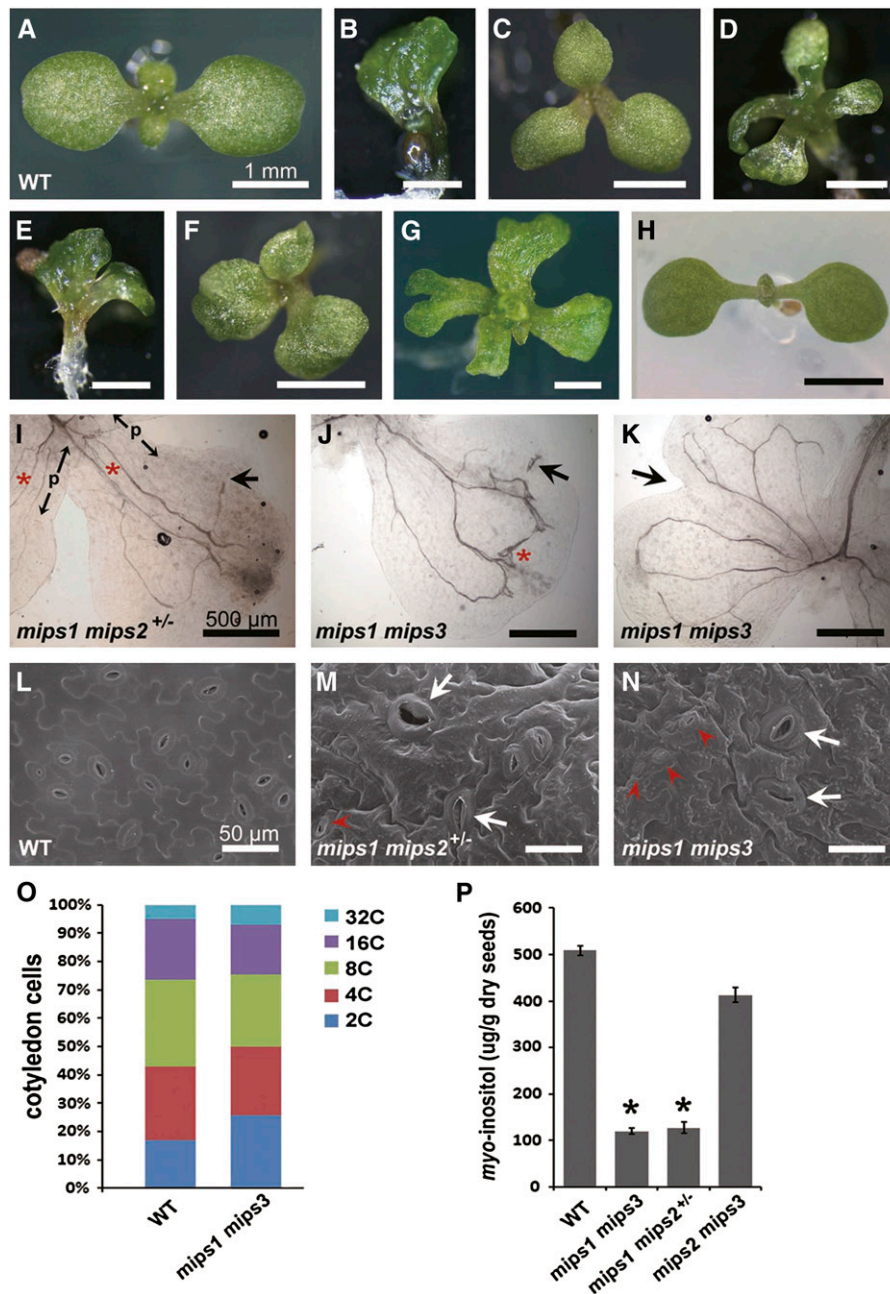
Figure 6. Phenotypic Analysis of *mips* Double Mutant Cotyledons.

(A) to **(H)** Cotyledon phenotypes of wild-type (WT; **[A]**), *mips1 mips2*^{+/−} (**[B]** to **[D]**), *mips1 mips3* (**[E]** to **[G]**), and the complementation line of *mips1 mips3* with genomic *MIPS1* gene driven by its own promoter **(H)**. Bars = 1 mm.

(I) to **(K)** The vascular patterns of cotyledons of *mips1 mips2*^{+/−} **(I)** and *mips1 mips3* (**[J]** and **[K]**). Red asterisks in **(I)** indicate the paralleled veins in cotyledon petioles, and the asterisk in **(J)** indicates irregular vein cluster. The arrow in **(I)** indicates the open end of a vascular bundle and in **(J)** indicates the isolated vascular segment. Cotyledon fusion site of *mips1 mips3* seedlings is indicated by arrow in **(K)**. P, petiole. Bars = 500 μm.

(L) to **(N)** Pavement cell and stomatal guard cell morphology of the wild-type **(L)**, *mips1 mips2*^{+/−} **(M)**, and *mips1 mips3* **(N)** double mutant cotyledons. Extremely large guard cells (arrows) and small guard cells (red arrowheads) were found in *mips* double mutant cotyledons. Bars = 50 μm.

(O) Relative cell ploidy ratio of the wild-type and *mips1 mips3* cotyledons. More than 10,000 nuclei were counted for each sample.

(P) *myo*-inositol content in mature seeds of wild-type and *mips* double mutants. Asterisks indicate P value <0.001. Error bars were calculated as SE for three independent experiments.

Table 1. Frequencies of Cotyledon Phenotypes from Seeds of a Single Plant of the Genotypes Listed

| | Cotyledon Nos. and Frequency | | | | | | |
| | | Two | | | | | |
Parental Genotype	One	Symmetry	Asymmetry	Three	Four	Ungerminated	Total No. of Seedlings
mips1 mips3 (1)	8	103	123	48	5	0	287
mips1 mips3 (2)	6	79	97	30	4	0	216
	2.8%	36.2%	43.7%	15.5%	1.8%		
mips1 mips2$^{+/-}$ (1)	7	17	23	9	1	9	66
mips1 mips2$^{+/-}$ (2)	14	40	30	12	0	18	114
	11.7%	31.7%	29.4%	1%	0.6%	15%	

The aborted seeds in *mips1 mips2$^{+/-}$* were excluded before plating on the half-strength Murashige and Skoog medium and were not counted as ungerminated. All the seedlings that were counted as *mips1 mips2$^{+/-}$* were genotyped. Numbers in parentheses represent the number of independent lines of each genotype.

that, unlike the wild type (Figure 6L), abnormal cotyledons of both *mips1 mips2$^{+/-}$* and *mips1 mips3* showed uneven cotyledon surfaces with unequal pavement cell and stomata cell sizes (Figures 6M and 6N). To investigate whether the abnormal size of the cotyledon epidermal cells was caused by endoreduplication (Melaragno et al., 1993), we conducted flow cytometry analysis on the cotyledon cells from *mips1 mips3* seedlings at 10 d after germination (DAG). The results showed that both 2C and 32C cells were more abundant in the *mips1 mips3* mutants than in the wild type (Figure 6O), suggesting that cell cycle regulation is affected in *mips1 mips3* cotyledon cells.

We used gas chromatography–time-of-flight–mass spectrometry (MS) to determine whether the *myo*-inositol content is indeed reduced in the mature seeds of the double mutants, since *MIPS* genes were highly expressed in the developing seeds (Figure 3). The result showed that, while the *myo*-inositol level in wild-type seeds was 509 ± 11 µg/g tissue, the *myo*-inositol contents in *mips1 mips3*, *mips1 mips2$^{+/-}$*, and *mips2 tmips3* double mutants were 120 ± 6 µg/g tissue, 127 ± 12 µg/g tissue, and 413 ± 16 µg/g tissue, respectively (Figure 6P). These results indicate that the *myo*-inositol level was indeed reduced in the higher-order *MIPS* mutants and that *MIPS1* is the most important member responsible for the *myo*-inositol synthesis in *Arabidopsis* seeds.

MIPS Genes Are Required for Embryo Development

Because the initiation of cotyledons begins at the late globular stage of embryo development (Chandler, 2008) and many mutants defective in embryo development also displayed abnormal cotyledons (Berleth and Jürgens, 1993; Bennet et al., 1995; Aida et al., 1997; Friml et al., 2003), we investigated embryo development in the double mutants. Whereas normal embryo development was observed in the wild type (Figures 7A to 7D), disorganized embryo basal shapes were observed in globular stage embryos of *mips1 mip2$^{+/-}$* (Figure 7E) and *tmips1 mips3* (Figure 7I). From the heart stage on, single and triple cotyledon primordia were visible in the double mutant *misp1 mips2$^{+/-}$* (Figures 7F and 7G). The *mips1 mips3* double mutant showed asymmetrical cotyledon primordia (Figure 7J) and abnormal

bulges in the hypocotyls (Figure 7K). Both of these double mutants produced abnormal mature embryos (Figures 7H and 7L).

We failed to obtain any *mips1 mips2* homozygous double mutants. Normal green round seeds developed in the wild-type siliques (Figure 7M), whereas in the siliques of *mips1 mips2$^{+/-}$*, we observed both green round seeds and white wrinkled seeds, with a ratio of $\sim$3:1 (525:191, $\chi^2 = 0.99$; P > 0.05; Figure 7N), suggesting that the *mips1 mips2* homozygous mutant is embryo lethal. Like *mips1 mips2$^{+/-}$*, approximately one-quarter of the seeds in siliques of the *mips1$^{+/-}$ mips2 mips3* triple mutant were white; the green-to-white ratio was 672:197 ($\chi^2 = 2.39$; P > 0.05; Figure 7O). These white embryos were at the late globular shape to heart shape stages. After the globular stage, the development of *mips1 mips2 mips3* mutant embryos was mostly arrested (Figures 7P and 7R), while *mips2 mips3* and *mips1$^{+/-}$ mips2 mips3* embryos from the same silique developed beyond the globular stage (Figures 7Q and 7S).

In summary, if *mips1* was heterozygous in the double mutant, then no embryo defective phenotype was observed. In the *mips1* homozygous background, plants heterozygous for *mips2* or, by contrast, homozygous for *mip3*, produced severe embryo defective phenotypes, whereas the homozygous *mips1 mips2* double mutant was embryo lethal (Table 2). Our data demonstrate that, among the three *MIPS* genes, *MIPS1* has the most important role during *Arabidopsis* embryo development.

Defective Embryo Development in *mips* Mutants Is Associated with Impaired Distribution and Polar Transport of Auxin

Symmetrical outgrowth of cotyledon primordia depends on appropriate apical auxin maxima. To investigate whether auxin distribution was affected in *mips* mutants, we crossed the *mips* double and triple mutants with the auxin reporter DR5:green fluorescent protein (GFP) and examined the GFP signals in the embryos. In the embryo of wild-type *Arabidopsis*, auxin accumulated in the uppermost suspensor cells (hypophysis) at the globular stage (Figure 8A) and in cotyledon primordial tips and prevascular cells at the heart and torpedo stages in addition to
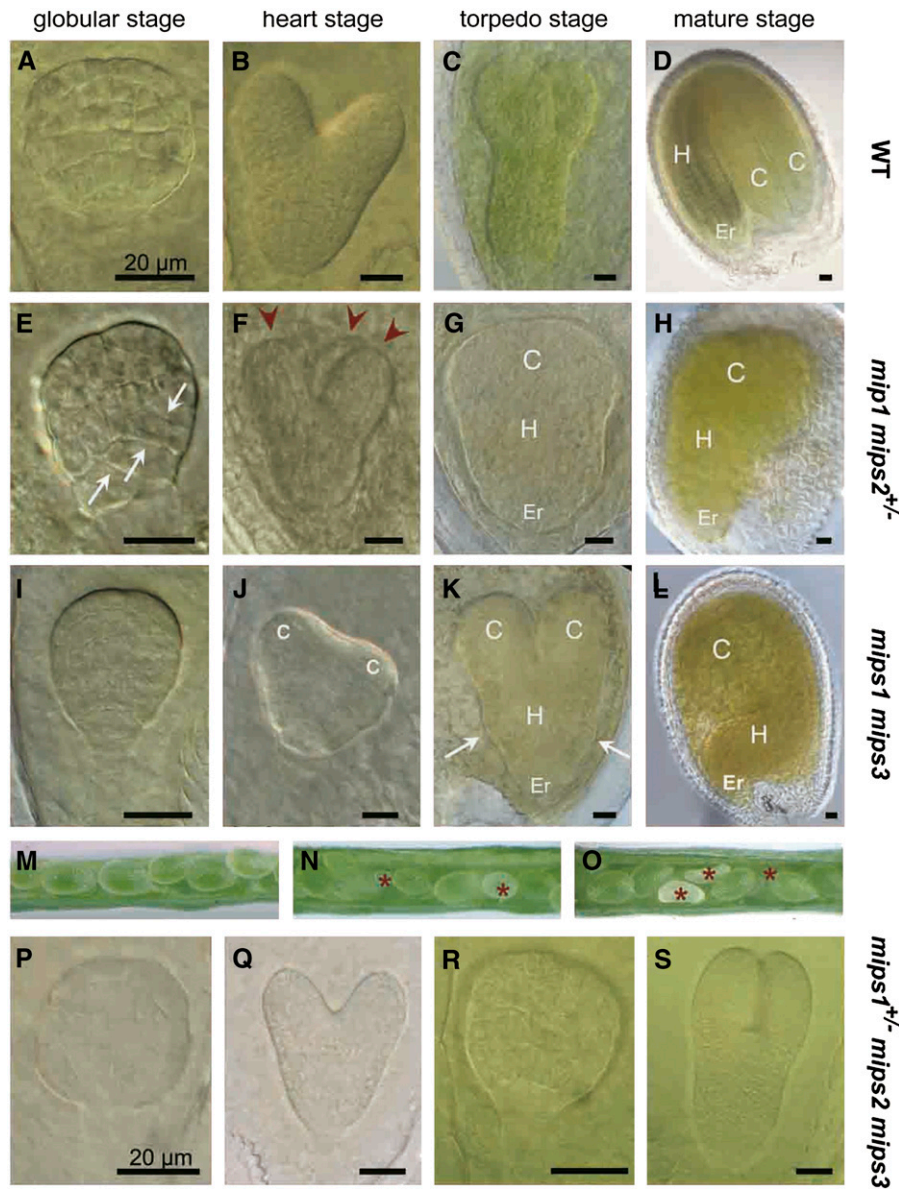
Figure 7. Embryo Development of the Wild Type and *mips* Double and Triple Mutants.

(A) to **(L)** Nomarski images of cleared *Arabidopsis* seeds from siliques of the wild type (WT; **[A]** to **[D]**), *mips1 mips2*$^{+/-}$ (**[E]** to **[H]**), and *mips1 mips3* (**[I]** to **[L]**) at the four developmental stages noted at the top of the figure. Arrows in **(E)** indicate the abnormal cell division orientation, and red arrowheads in **(F)** indicate three cotyledon primordia. The arrow pair in **(K)** indicates the abnormal bulges in hypocotyl. C, cotyledon primordium; H, hypocotyl; Er, embryonic root. Bars = 20 μm.

(M) to **(O)** Dissected siliques of the wild type **(M)**, *mips1 mips2*$^{+/-}$ **(N)**, and *mips1*$^{+/-}$ *mips2 mips3* **(O)**. Red asterisks indicate the flat white seeds that are distinguishable from the adjacent round green seeds.

(P) to **(S)** Nomarski images of cleared *Arabidopsis* seeds from *mips1*$^{+/-}$ *mips2 mips3* siliques. In one silique, although most of the embryos reached the heart stage **(Q)**, about a quarter of the embryos remained at the globular stage **(P)**. When most of the embryos reached the torpedo stage **(S)**, about a quarter of the embryos from the same silique remained at the globular stage **(R)**. Bars = 20 μm.

the hypophysis (Figures 8B and 8C), consistent with previous reports (Tanaka et al., 2006; Chandler, 2008; Nawy et al., 2008). In the embryos from *mips1 mips2*$^{+/-}$ siliques, in addition to the signal from the uppermost hypophysis, we observed an extra signal from suspensor cells at the late globular stage (Figure 8D).

At the heart stage, asymmetrical auxin maxima were observed in cotyledon primordia, although the embryo was morphologically symmetrical (Figure 8E). In most of the *mips1 mips2*$^{+/-}$ mature embryos, an apical expression pattern of DR5:GFP signal was observed (Figure 8F). In *mips1 mips3* embryos, a very weak DR5:

Table 2. The Phenotypes of *mips* Single, Double, and Triple Mutants under Optimal Growth Conditions

Genotype	Embryo Phenotype	Postembryo Phenotype
mips1	No	No
mips2	No	No
mips3	No	No
mips2 mips3	No	No
mips1 mips3	Deformed embryo	Dwarf and small; anthocyanidin accumulation
mips1⁺/⁻ mips2	No	1/4 Bearing seeds aborted
mips1 mips2⁺/⁻	Deformed embryo; ungerminated seeds	Leaf PCD; 1/4 bearing seeds aborted
mips1 mips2	Embryo lethal	NA
mips1⁺/⁻ mips2 mips3	No	1/4 Bearing seeds aborted
mips1 mips2⁺/⁻ mips3	Deformed embryo	Fragile; small; anthocyanidin accumulation
mips1 mips2 mips3	Embryo lethal	NA

Seedling phenotypes of some double and triple *mips* mutants are shown in Supplemental Figure 3 online. NA, not applicable.

GFP signal was observed in the hypophysis (Figure 8G). Meanwhile, auxin distribution was severely altered (e.g., globular-shaped *mips1 mips3* embryos at the heart or torpedo stages showed two auxin level peaks) (Figure 8H), and a bulged embryo proper showed dispersed GFP signals (Figure 8I). In all the embryos of *mips1 mips2⁺/⁻* and *mips1 mips3*, we detected GFP signals at the root pole (Figures 8F and 8I). Interestingly, we observed distorted distribution of the GFP signals in the *mips1 mips2 mips3* embryos dissected from mature siliques of *mips1⁺/⁻ mips2 mips3*. This result suggested that the cells are alive, even though the embryo development had ceased and that the distribution of auxin was greatly distorted (Figures 8J to 8L). The fact that the aberrant DR5:GFP signals were observed before the asymmetrical morphology emerged in the embryos
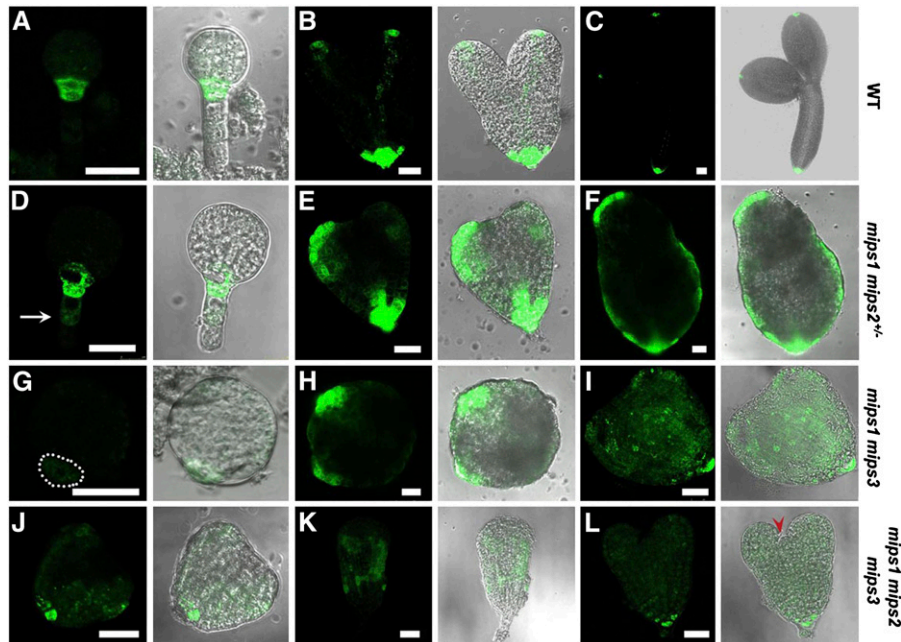

Figure 8. Auxin Maxima Distribution in the Wild-Type, *mips* Double, and Triple Mutant Embryos.

(A) to **(C)** DR5:GFP distribution in the wild-type (WT) embryos at the globular stage **(A)**, the late heart stage **(B)**, and the mature stage **(C)**.
(D) to **(F)** DR5:GFP distribution in embryos dissected from *mips1 mips2⁺/⁻* siliques at the globular stage **(D)**, the late heart stage **(E)**, and the mature stage **(F)**. Arrow in **(D)** indicates the extra GFP signal in suspensor cells.
(G) to **(I)** DR5:GFP distribution in *mips1 mips3* embryos at the globular stage **(G)**, the late heart stage **(H)**, and the torpedo stage **(I)**. The dashed line frame in **(G)** indicates the hypophysis cells with decreased DR5:GFP signals.
(J) to **(L)** DR5:GFP distribution in embryos dissected from the flat white seeds of *mips1⁺/⁻ mips2 mips3* mature silique (**[J]** and **[K]**). Red arrowhead in **(L)** indicates the abnormal bulge in shoot apical meristem.
Bars = 25 μm in **(A)** to **(L)**.

suggests that auxin distortion is probably responsible for abnormal embryo development.

PIN1 Localization Was Altered in *mips* Mutant Embryos

The correct establishment and maintenance of auxin maxima is important for normal bilateral axis formation in *Arabidopsis* embryos. These processes rely on the polar localization of the auxin efflux carrier, PIN1. Incorrect localization of PIN1 can result from cytoskeleton disruption and changes in the sterol component of the plasma membrane (Kleine-Vehn and Friml, 2008). To investigate whether PIN1 localization was altered in mutant embryos, we crossed *mips1 mips2*$^{+/-}$ and *mips1 mips3* double mutants with a PIN1:GFP marker line. At the globular stage, PIN1:GFP was expressed in the epidermal cells in *mips1 mips2*$^{+/-}$ and *mips1 mips3* embryos, similar to the expression in the wild type. However, whereas PIN1 showed polar plasma membrane localization in the wild-type embryo (Figure 9A), localization of PIN1:GFP was less polar in the *mips1 mips2*$^{+/-}$ embryos (Figure 9B) and localized at two opposite membranes (Figure 9C) or outward membranes of epidermal cells (Figure 9D) in *mips1 mips3* embryos. Within the same silique of *mips1 mips2*$^{+/-}$, we found later-stage embryos of *mips1*, *mips1 mips2*$^{+/-}$, and *mips1 mips2* in which PIN1 localization differed (Figures 9E to 9G). These data suggest that PIN1 polar localization was altered in the mutant embryos at the globular stage. Because at this stage most of the double mutant embryos showed normal morphology with no apical DR5:GFP signals, it is likely that the altered PIN1 localization at the globular stage is responsible for distorted apical auxin distribution at later developmental stages.

Embryo-Defective Phenotypes of *mips* Double Mutants Are Rescued by *PIS* Overexpression but Enhanced by *UGT84B1* Overexpression

After synthesis, *myo*-inositol, together with CDP-diacylglycerol, can be converted to PtdIns in a reaction catalyzed by PIS1 and PIS2 (Collin et al., 1999). To clarify the primary defects caused by *myo*-inositol deficiency, we cloned *PIS1* and *PIS2*, generated overexpression constructs driven by their native promoters plus four cauliflower mosaic virus 35S enhancers, and transformed these constructs into both the *mips1 mips3* double mutant and the wild type. In the *PIS2* overexpressor lines in the *mips1 mips3* background, plants with two normal symmetric cotyledons accounted for >65% of the population, compared with 36% in *mips1 mips3*, indicating that *PIS2* overexpression had largely rescued the cotyledon symmetry phenotypes in the *mips1 mips3* double mutants (Figures 10A and 10B, Table 3). Moreover, *PIS1* overexpression partially rescued the cotyledon phenotype of *mips1 mips3* double mutants but not the short-root phenotype (Figures 10C and 10D, Table 3). By contrast, overexpression of *PIS2* or *PIS1* in wild-type plants did not affect the cotyledons (Figure 10E). Moreover, recent studies showed that the levels of PtdIns species were reduced in *mips1* single mutants (Chen and Xiong, 2010; Donahue et al., 2010). These results suggest that the defects in *mips* mutants were caused by decreased levels of PtdIns and that *myo*-inositol synthesized by MIPS is essential for synthesis of PtdIns.

In maize, *myo*-inositol can also be conjugated with IAA to form *myo*-inositol–conjugated IAA molecules. We then generated *UGT84B1* overexpression constructs driven by their native promoters plus four cauliflower mosaic virus 35S enhancers and transformed these constructs into both the *mips1 mips3* double mutant and the wild-type *Arabidopsis* plants. In contrast with *PIS* overexpressor lines, most of the *UGT84B1* overexpressor lines in the *mips1 mips3* mutant background exhibited stronger cotyledon phenotypes, and some developed no roots (Figures 10F and 10G), whereas overexpression of *UGT84B1* in wild-type plants did not affect the cotyledons (Figure 10H). Since there is no report of the existence of IAA-*myo*-inositol in *Arabidopsis* up to now, we first adopted HPLC-MS to clarify this question. The result showed that four IAA-*myo*-inositol isomers existed both in *Arabidopsis* roots and siliques (the data of *mips1 mips3* are shown as an example), while two isomers existed in maize kernels, by comparing the chromatogram and spectra with those of chemically synthesized IAA-*myo*-inositol (Figures 10I and 10J). Then, we performed the relative quantification analysis on the roots from germinating seeds of the wild type, *mips 1 mips3* double mutants, and *UGT84B1* overexpressor lines using HPLC-MS. The result showed that overexpression of *UGT84B1* in the *mips1 mips3* background resulted in a significant increase in IAA-*myo*-inositol level, whereas the relative level of the IAA-*myo*-inositol content in *mips1 mips3* double mutant was slightly lower than the wild type (Figure 10K). It is possible that the more severe cotyledon phenotypes in the *UGT84B1* overexpressor lines in the *mips1 mips3* background are attributed to the further reduction of the free *myo*-inositol in the mutant, which suggests the essential role of free *myo*-inositol in cotyledon development. Another possibility is that increase of the IAA-*myo*-inositol level also further reduced the level of free active IAA, the distribution and transport of which had already been severely distorted in the mutant (Figures 8 and 9), which further confirmed the role of auxin distortion as the major factor that causes the abnormal cotyledon phenotypes in the *mips* mutants.

Endomembrane Function in Embryo Cells Was Impaired in the *mips1 mips3* Double Mutant

We first used the endomembrane trafficking inhibitor brefeldin A to analyze PIN1:GFP trafficking in both the wild type and *mips1 mips3* double mutant. However, the PIN1 proteins abnormally aggregated in *mips1 mips3* embryo cells even without brefeldin A treatment (see Supplemental Figure 4 online), suggesting that the PIN1 trafficking in the double mutant embryo cells was affected, possibly due to the impaired PIN1 exocytosis. To investigate whether the endomembrane function is affected, we then used the fluorescent styryl dyes (e.g., FM4-64 and FM1-43) to either mark the plasma membrane or monitor the clathrin-dependent endocytosis process (Bolte et al., 2004) in *mips* double mutant embryo cells at early stages. After treatment, the dye first stains the plasma membrane, then reaches the endosomal network through endocytic internalization, and finally labels the surface of vacuole (Ueda et al., 2001). We used the dye AM1-43, the fixable form of FM1-43 with similar emission
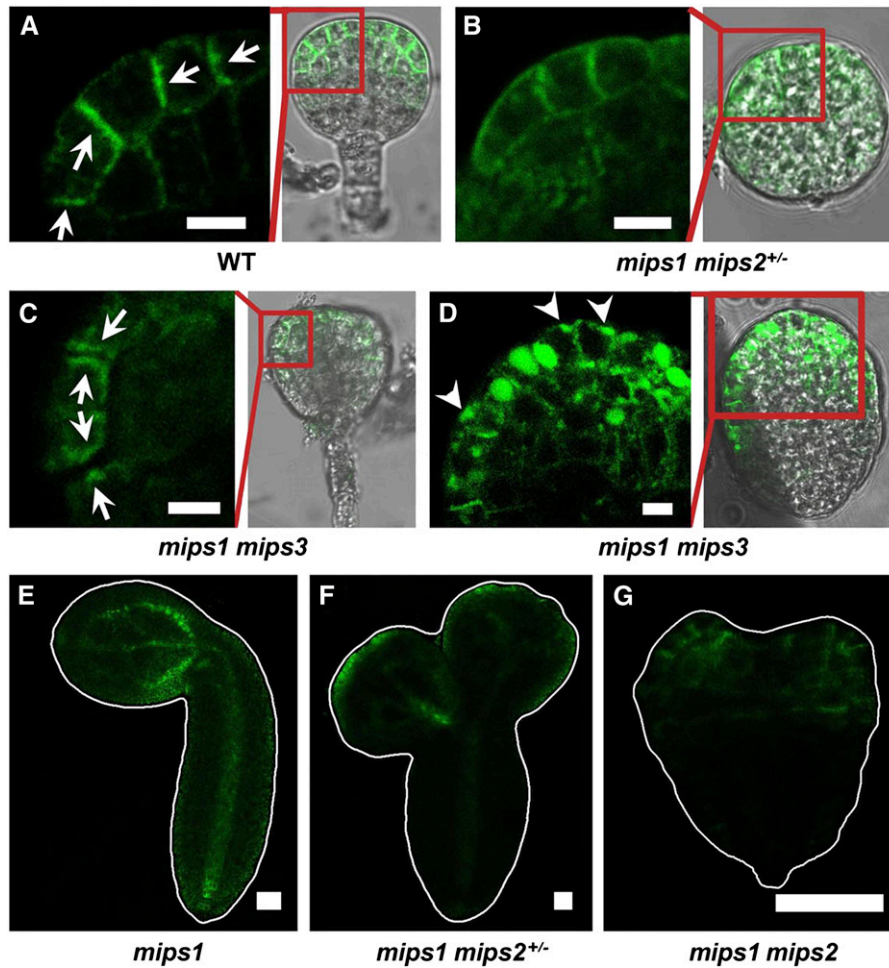
Figure 9. PIN1 Localization in the Wild-Type and *mips* Double Mutant Embryos.

(A) PIN1:GFP signals in a globular stage embryo of the wild type (WT). Arrows show the PIN1:GFP polar localization, which indicates the direction of auxin flux toward the differentiating cotyledon primordium.

(B) A globular shape embryo dissected from a silique of *mips1 mips2*$^{+/-}$ showing evenly distributed PIN1:GFP signals on plasma membrane.

(C) and **(D)** PIN1:GFP signals in globular-stage embryo of *mips1 mips3*. Arrows in **(C)** indicate the disorganized PIN1 localization on lateral plasma membranes. Arrowheads in **(D)** indicate PIN proteins facing outwards. In **(A)** to **(D)**, the left panels show the fluorescence image of the area in the red rectangle in the right Nomarski image. Bars = 5 μm in **(A)** to **(D)**.

(E) to **(G)** Three phenotypically distinct embryos dissected from the same silique of *mips1 mips2*$^{+/-}$ showing different PIN1:GFP signals. The predicted genotypes are *amips1* **(E)**, *mips1 mips2*$^{+/-}$ **(F)**, and *mips1 mips2* **(G)**. Bars = 25 μm.

and absorption spectra, for the assay. The results showed that, in the embryo cells at the globular stage, after 5-min treatment, AM1-43 dye was extensively endocytosed and was detectable in the vacuole membrane in the wild type (Figure 11A) but not in *mips1 mips3* mutants (Figure 11D). Most of the globular embryo cells of *mips1 mips3* remained in the plasma membrane (Figure 11D). In the embryo cells at the early heart stage, 5-min treatment produced dye-stained vesicles in the wild type (Figure 11B), while mutant cells had much less stained vesicles (Figures 11B and 11E). The fact that the dye uptake rate is slower in the mutant suggests that the endocytosis is affected in the mutant embryo cells. After 10-min treatment, the dye was endocytosed completely into the cells and trafficked to the vesicle membrane both

in the wild type and the mutant (Figures 11C and 11F). Interestingly, some *mips1 mips3* embryo cells showed a massive intake of the fluorescent dye (Figure 11F), implying that the integrity of the plasma membrane is also impaired in the mutant embryo cells (Schapire et al., 2008).

To investigate whether the endomembrane structure was affected in the *mips1 mips3* double mutant, we carefully analyzed the endomembrane structures in torpedo stage embryos of the wild type and *mips1 mips3* double mutant by transmission electron microscopy. Compared with those of the wild type (Figure 11G), the vesicle budding structures were much less prominent in *mips1 mips3* (Figure 11I). Single-layer vesicles were commonly found in wild-type embryo cells (Figure 11H) but were
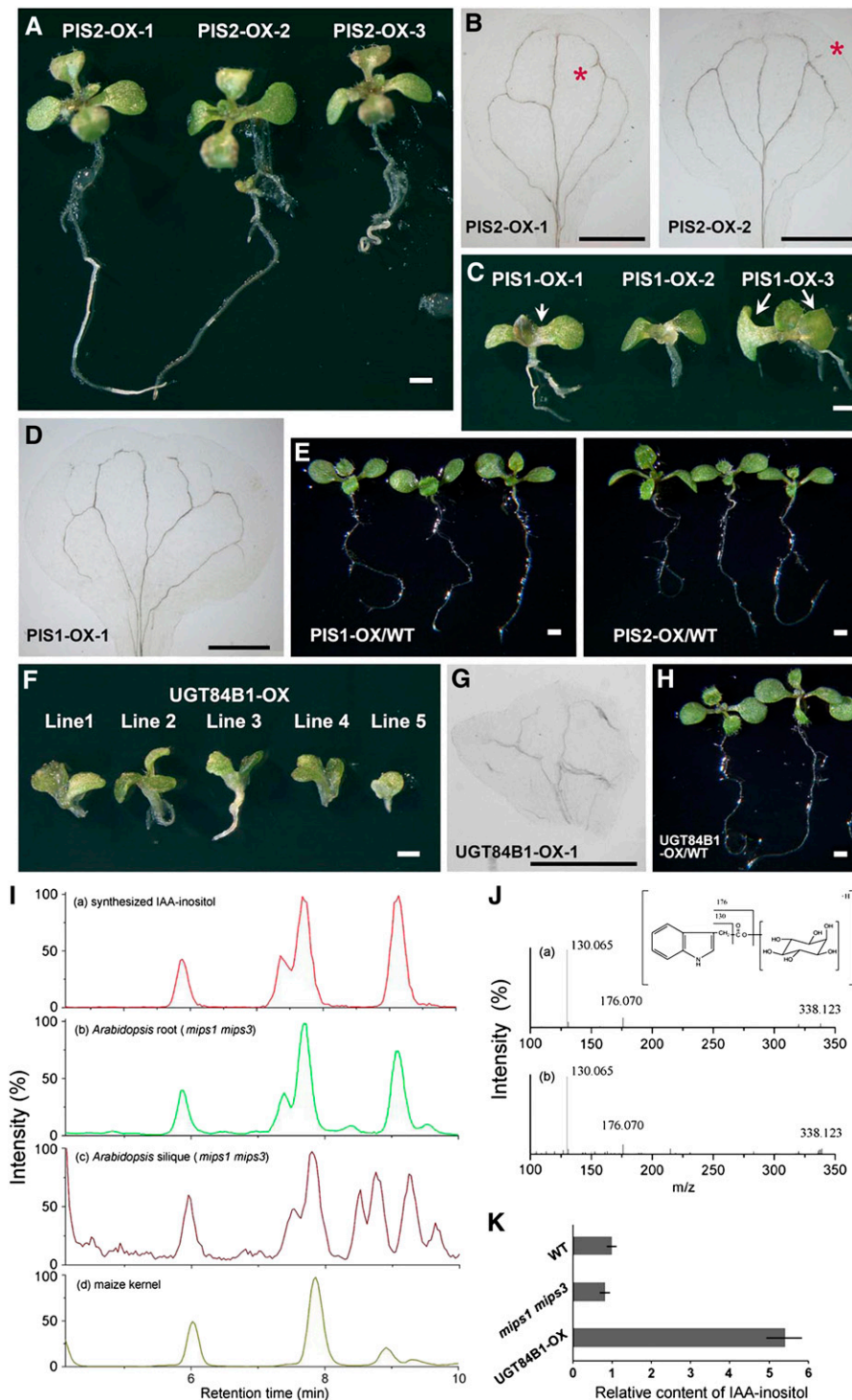
Figure 10. Phenotypic Analysis and Biochemical Characterization of *PIS2*-, *PIS1*-, and *UGT84B1*-Overexpressor Lines in the *mips1 mips3* Background.

(A) to **(H)** The 12-DAG PIS2-OX **(A)**, PIS1-OX **(C)**, and UGT84B1-OX **(F)** transgenic lines in the *mips1 mips3* background. The T1 generation lines shown above were selected by growing on half-strength Murashige and Skoog agar plate containing 50 μg/mL hygromycin. PIS2-OX lines in **(A)** show regularly symmetry two cotyledons. Arrow (left) in **(C)** indicates the broader cotyledon petiole; arrow pair (right) in **(C)** indicates the two asymmetric cotyledons. Cotyledon venations of PIS2-OX **(B)**, PIS1-OX **(D)**, and UGT84B1-OX **(G)** transgenic lines. Red asterisks in **(B)** indicate the extra vascular structures. Wild-type *Arabidopsis* overexpressing *PIS2* (PIS2-OX) or *PIS1* (PIS1-OX) **(E)** or *UGT84B1* (UGT84B1-OX) **(H)** are also shown. Bars = 1 mm.

Table 3. Frequencies of Cotyledon Phenotypes from Seeds of Single Plants

| Parental Genotype | Cotyledon Nos. and Frequency | | | | | |
| | One | Two | | Three | Four | Total No. of Seedlings |
		Symmetry	Asymmetry			
PIS2-OX-1	2	83	7	3	0	95
	2.1%	87.4%	7.4%	3.2%		
PIS2-OX-2	5	61	18	9	0	93
	5.4%	65.6%	19.8%	9.7%		
PIS2-OX-3	1	68	19	7	0	95
	1.1%	71.6%	20.0%	7.4%		
PIS1-OX-1	4	42	36	12	0	94
	4.3%	44.7%	37.5%	12.5%		
PIS1-OX-2	2	55	22	10	0	89
	2.3%	61.8%	24.7%	11.2%		
PIS1-OX-3	3	38	31	9	0	81
	3.7%	46.9%	38.3%	11.1%		

A single transgenic plant was used for statistical analysis of each transgenic line.

rarely observed in *mips1 mips3* (Figure 11J; see Supplemental Figure 5 online). These data, together with the AM1-43 staining results, suggest that both the endomembrane trafficking process and the endomembrane structure were damaged in *mips1 mips3*. This hypothesis is further supported by the complementation result that these vesicles were restored in the *mips1 mips3* mutant embryos when *PIS2* was overexpressed (Figures 11K and 11L; see Supplemental Figure 5 online). Since PIN1 polar localization depends on polar trafficking of recycled endosomes, which is initiated by endocytosis from the plasma membrane (Kleine-Vehn and Friml, 2008), the defective polar localization of PIN1 in the *mips* embryos could therefore be attributed to the defects in membrane dysfunction caused by the lack of *myo*-inositol.

In conclusion, our study showed that MIPS-catalyzed de novo synthesis of *myo*-inositol is essential for auxin-mediated embryo development in *Arabidopsis*. The *myo*-inositol serves as the main substrate for synthesis of PtdIns, the membrane component essential for keeping normal function of endomembrane trafficking and maintenance of endomembrane structure, which is critical for the correct auxin transport and, thus, correct auxin localization during embryo pattern formation (Figure 12).

DISCUSSION

In this study, we demonstrated distinct dynamic expression patterns of three *MIPS* genes that are essential for normal *Arabi*-

dopsis embryo development. Moreover, we provided evidence for the direct involvement of PtdIns, a derivative of *myo*-inositol, in auxin-regulated embryo pattern formation.

Although previous studies on other plant species revealed high levels of expression of *MIPS* genes during seed development (Johnson and Wang, 1996; Yoshida et al., 1999; Hegeman et al., 2001; Abreu and Aragão, 2007), the exact function of *MIPS* in this process remains elusive, possibly because of the multiple copies of *MIPS* genes in plants. For instance, in *Arabidopsis*, the detailed expression pattern of each of the MIPS proteins was difficult to distinguish in developing seeds because of the high amino acid sequence identity among the three MIPSs. In this study, we found that *MIPS1* was expressed at all stages during embryo development. By contrast, expression of *MIPS2* and *MIPS3* was detected in the seed coat and funiculus of maternal tissues after the globular stage (Figure 3) but decreased to undetectable levels in the embryo and endosperm. The overlapping expression of the three *MIPS* genes at the globular stage, but not at later stages, suggests an essential role of *myo*-inositol synthesis at early stages of embryo development. As embryo development proceeds, it is likely that MIPS1 alone synthesizes sufficient *myo*-inositol for the later embryo stages. The fact that a complete knockout of *MIPS1* showed no phenotype during the entire process of embryo development suggests that the amount of *myo*-inositol synthesized by both MIPS2 and MIPS3 at the globular stage is sufficient for normal embryo development. Expression of *MIPS2* and *MIPS3* in the endosperm and maternal tissues after the globular stage provides another route by which

Figure 10. (continued).

(I) Liquid chromatography–MS chromatograms of IAA-*myo*-inositol quantification assay using synthesized IAA-*myo*-inositol **(a)**, *mips1 mips3* root **(b)**, *mips1 mips3* silique **(c)**, and maize kernel **(d)**. Four peaks in chromatogram **(a)** show four isomers of IAA-*myo*-inositol.

(J) MS^2 spectra of the first isomer (retention time, 5.9 min) in synthesized IAA-*myo*-inositol **(a)** and wild-type *Arabidopsis* root **(b)**. The fraction of *m/z* 130 and *m/z* 176, as well as the [M+H]$^+$ *m/z* 338.123, confirmed the IAA-*myo*-inositol structure of the first isomer.

(K) Relative content of IAA-*myo*-inositol in *Arabidopsis* root tissue of different genotypes. Duplicate experiments were performed for each genotype. Error bars show SE. WT, wild type.
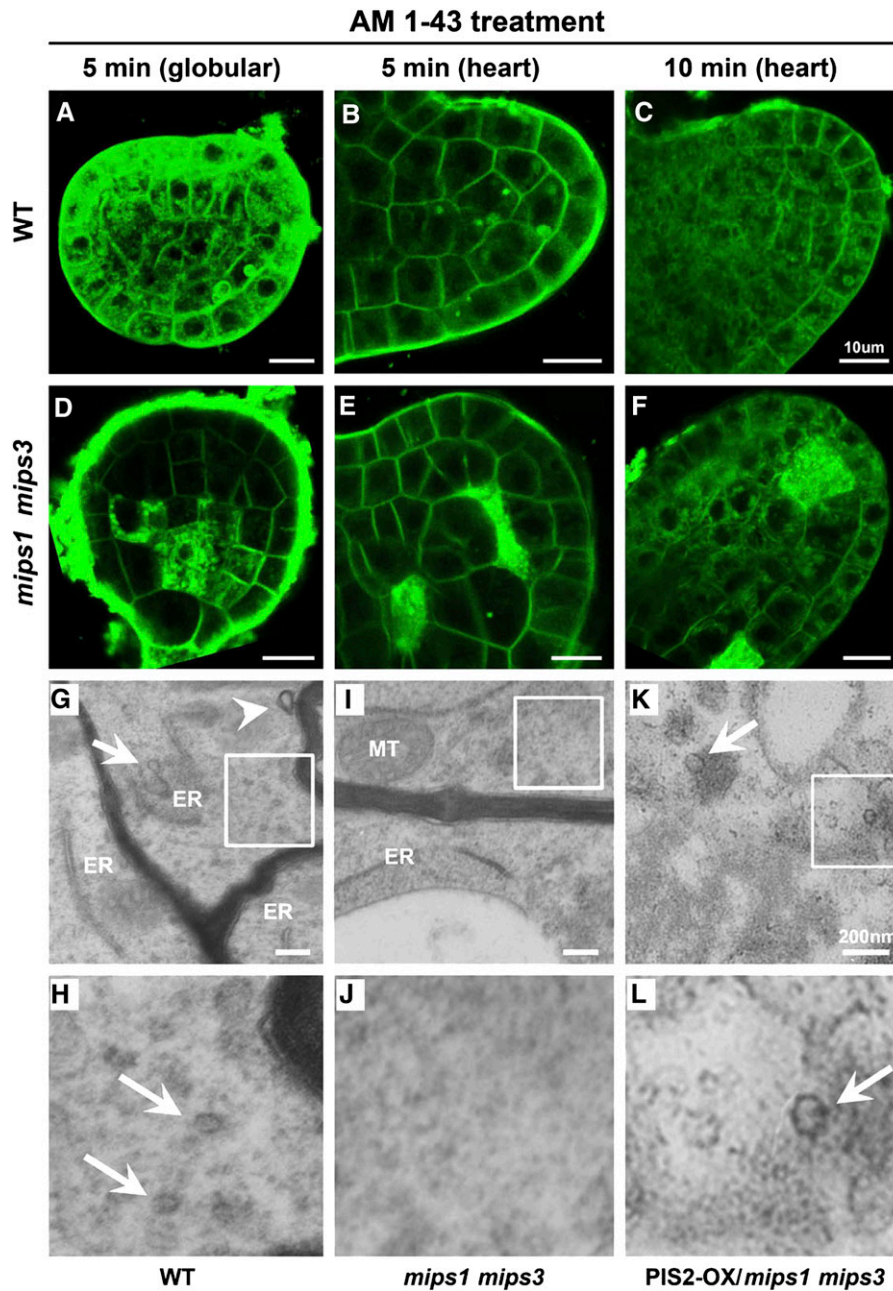
Figure 11. Endomembrane of the Wild-Type and *mips1 mips3* Embryo Cells.

(A) to **(F)** *Arabidopsis* wild-type (WT; **[A]** to **[C]**) and *mips1 mips3* double mutant (**[D]** to **[F]**) embryo cells treated with the endocytosis marker AM1-43. More than 20 siliques were analyzed for each treatment. Bars = 10 μm.

(G) Endomembrane system of a wild-type embryo cell at the torpedo stage. Arrowhead indicates a double membrane bound vesicle; arrow indicates a budding vesicle. ER, endoplasmic reticulum. Bar = 200 nm.

(I) Endomembrane system of an *mips1 mips3* embryo cell at the torpedo stage. MT, mitochondria. Bar = 200 nm.

(K) Endomembrane system of a torpedo embryo cell from PIS2-OX–transformed *mips1 mips3* plant; arrow indicates a trafficking vesicle. Bar = 200 nm.

(H), **(J)**, and **(L)** Magnification of rectangle regions in **(G)**, **(I)**, and **(K)**, respectively. Arrows in **(H)** and **(L)** indicate the single membrane bound trafficking vesicles, which were not found in **(J)**.
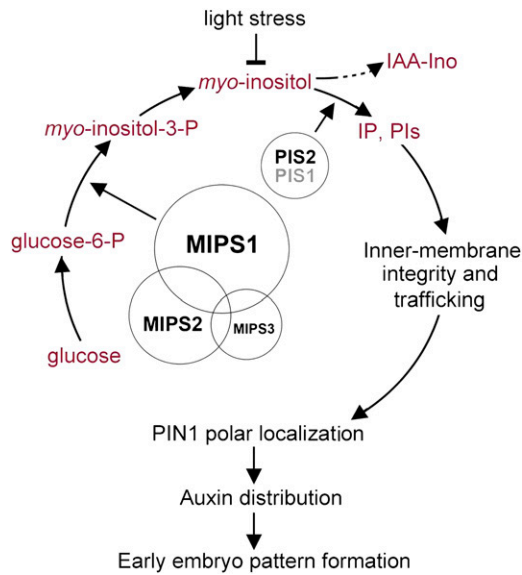
Figure 12. A Proposed Model for the Biological Roles of the Three *MIPS* Genes in *Arabidopsis* Embryo Pattern Formation.

The *myo*-inositol produced by sequential reactions, in which MIPS enzymes catalyze the rate-limiting step, can be either conjugated to IAA or converted to membrane component PtdIns. Sufficient PtdIns is important for endomembrane structure and trafficking and, thus, for auxin transport and localization to regulate proper embryo development.

the *myo*-inositol synthesized in the endosperm and maternal tissues can be transported to the embryo. The double mutants *mips1 mips2*$^{+/-}$ and *mips1 mips3* displayed impaired embryo symmetry after the late globular stage, whereas the embryo development of *mips2 mips3* was normal. This result indicates that *MIPS1* plays the most important role in synthesizing *myo*-inositol for embryo development, consistent with the high expression levels of *MIPS1* at all stages of embryo development. It appears that *MIPS2* has a more important role in embryo development than *MIPS3* because *MIPS2* had a broader expression pattern than that of *MIPS3* (Figure 3), and the *mips1 mips2* double mutant is embryo lethal. In addition to the production of phytate in seed phosphorus and cation storage (Brinch-Pedersen et al., 2002; Stevenson-Paulik et al., 2005), here, we used genetic approaches to demonstrate that the coordinated expression of the three *MIPS* genes is also essential for embryo pattern formation in *Arabidopsis*.

myo-inositol is transformed into various derivatives that have roles in numerous biological pathways. In mammalian systems, *myo*-inositol–derived molecules have two major roles: one as membrane components (i.e., PtdIns and PIs) and the other in signal transduction (i.e., inositol phosphates). However, the Ins (1,4,5)P$_3$ intracellular signal transduction pathway appears to be absent from plants, since no Ins(1,4,5)P$_3$ receptor has been found in land plants (Wheeler and Brownlee, 2008). On the other hand, *myo*-inositol can be conjugated with IAA to form *myo*-inositol–conjugated IAA molecules in *Arabidopsis* (Figure 10). The DR5:GFP (Figure 8) and PIN1:GFP (Figure 9) signals were severely altered in the embryos of *mips1 mips2*$^{+/-}$ and *mips1*

mips3, indicating that there is a connection between *myo*-inositol and auxin maxima/transport. Once produced, *myo*-inositol is transformed into different derivatives with roles in various biochemical processes and pathways. Therefore, the phenotypes caused by *myo*-inositol deficiency could result from many affected pathways. In this study, we used genetic and microscopy approaches to clarify which pathway(s) is most affected and to determine how *myo*-inositol production is associated with auxin during embryo development. Interestingly, we found that overexpression of *PIS2*, driven by its own promoter plus four 35S enhancers, largely rescued the cotyledon phenotype of *mips1 mips3* (Figure 10). Recently it was reported that overexpression of *PIS2* in *Arabidopsis* increased levels of PtdIns(4)P and PtdIns (4,5)P$_2$, which are the major PI species in plasma membranes, the endoplasmic reticulum, the Golgi complex, and trafficking vesicles (Löfke et al., 2008). Therefore, these results suggest that, under *myo*-inositol insufficient conditions, there are limited amounts of the membrane components PtdIns and PIs, possibly PtdIns(4)P and PtdIns(4,5)P$_2$. Defects in membrane function resulting from the limited amounts of membrane components might be the major reason for the embryo defects in *mips1 mips3*. Overexpression of *PIS2* would transform the limited amount of *myo*-inositol into PtdIns, thereby maintaining the membrane function and consequently largely rescuing the cotyledon phenotype. As a major component of nonphotosynthetic membranes, PtdIns and their phosphorylated forms, PIs, are involved in intracellular vesicular transport and function as the organelle identity markers. Each distinct organelle membrane has its unique PI composition (Simonsen et al., 2001; Krauß and Haucke, 2007). Our conclusion that endomembrane function was affected in *mips* mutants is supported by the transmission electron microscopy observation that the structures of inner membrane systems were altered, and there were significantly fewer membrane-derived trafficking vesicles in cells of *mips1 mips3*, which was largely rescued by the overexpression of *PIS2* (Figure 11). The lack of vesicle budding and trafficking could also explain the depolarization and mistransport of PIN:GFP in *mips* double mutant embryos.

Although *Arabidopsis* PIS1 and PIS2 share 87% identity at the amino acid level, overexpression of *PIS1* only partially rescued the cotyledon phenotype of *mips1 mips3*, while overexpression of *PIS2* more completely rescued it. One explanation could be that *PIS2* is specifically expressed in developing seeds but PIS1 is not, according to the microarray data (Zimmermann et al., 2004). Another possibility is that PIS1 and PIS2 have different biochemical properties because overexpression of *PIS1* did not affect PI content (Löfke et al., 2008).

Recently, the single knockout mutant *mips1* was reported to display leaf PCD and seed phenotype (Meng et al., 2009; Donahue et al., 2010). However, we did not observe any differences between the wild type and the *mips* single mutant (SALK_023626) under our experimental conditions (120 μmol m^{-2} s^{-1}, 16 h light/8 h dark). Our result is consistent with a previous report in which no developmental defects were observed in the *mips1* single mutant (Murphy et al., 2008). However, we observed stable occurrence of PCD patches in the *mips1 mips2*$^{+/-}$ leaves under the same (120 μmol m^{-2} s^{-1}, 16 h light/8 h dark) growth condition (see Supplemental Figure 3 online).

Furthermore, our light intensity experiment results showed that both rosette leaf and embryo development of *mips1* were sensitive to high light conditions, suggesting that the leaf PCD phenotype is attributed to the coaction of high light intensity stress and partial lack of the major MIPS activity. This hypothesis is further supported by a recent report that stress-induced reactive oxygen species would greatly reduce the cellular *myo*-inositol content without affecting the expression of *MIPS1* gene. Notably, the embryo phenotypes of *mips* double and triple mutants in our study were inheritably stable and were less affected by environmental factors, making them good materials for further genetic and cellular analysis.

In summary, we demonstrate that *myo*-inositol is the main substrate for synthesis of PtdIns, which are essential to maintain endomembrane function during embryo development. De novo synthesis of *myo*-inositol is required for the correct transport and localization of auxin during embryo pattern formation in *Arabidopsis*. Our findings suggest that there is a link between the lipid components and the dynamic function of endomembrane system.

METHODS

Yeast Complementation Assay

The yeast *ino1* strain SJY425 (*MATα his3Δ1 leu2Δ0 lys2Δ0 ura3Δ0 ino1Δ::HIS3MX6*) was kindly provided by Susan A. Henry (Nunez et al., 2008). *Arabidopsis thaliana MIPS1*, *MIPS2*, and *MIPS3* and yeast *INO1* genes were cloned into the yeast expression vector pAG425GPD-ccdB (*Saccharomyces cerevisiae* Advanced Gateway Destination vector from Addgene) (Alberti et al., 2007), and recombinants were transformed into *ino1* with *leu2* as the selection marker. The yeast synthetic complete medium contained the following ingredients per 1 liter double-distilled water: 20 g glucose, 5 g ammonium sulfate, 1 g potassium phosphate, 0.5 g magnesium sulfate, 0.1 g sodium chloride, 0.1 g calcium chloride, 0.5 mg boric acid, 0.04 mg cupric sulfate, 0.1 mg potassium iodide, 0.2 mg ferric chloride, 0.4 mg manganese sulfate, 0.2 mg sodium molybdate, 0.4 mg zinc sulfate, 2 µg biotin, 400 µg calcium pantothenate, 2 µg folic acid, 400 µg niacin, 200 µg *p*-aminobenzoic acid, 400 µg pyridoxine hydrochloride, 200 µg riboflavin, 400 µg thiamine, 20 mg adenine sulfate, 20 mg Arg, 20 mg His, 60 mg Leu, 230 mg Lys, 20 mg Met, 300 mg Thr, 20 mg Trp, and 40 mg uracil. In this experiment, Leu was omitted from the yeast synthetic complete medium. When transformed yeast cell suspensions reached 0.5 OD_{600}/mL, they were serially diluted (1:10) and spotted onto plates either with or without 75 µM *myo*-inositol. Plates were incubated at 30°C for 2 d before analysis.

Expression Analysis

Total RNA was isolated from wild-type seedlings grown on solid half-strength Murashige and Skoog medium under continuous light conditions at 8 DAG and from tissues of 30-DAG wild-type plants grown under 16-h-light/8-h-dark conditions using TRIzol reagent (Invitrogen) followed by RNase-free DNase (TaKaRa) treatment. For each sample, 500 ng RNA was reverse transcribed into cDNA using Superscript II reverse transcriptase (Invitrogen). Two microliters of diluted cDNA samples (1:10) were mixed with 10 µL SYBR Green Real-Time PCR Master Mix (TOYOBO) and 100 nM gene-specific primers that were designed from sequences close to the 3′ end (see Supplemental Table 1 online), and then quantitatively analyzed by an Opticon continuous fluorescence detector (MJ Research) (Liu et al., 2008). Three biological replications were performed for each template and primer combination, and *TUB2*

expression level was used as the internal control. We used the cycle threshold (Ct) $2^{-\Delta\Delta Ct}$ method (Livak and Schmittgen, 2001) to calculate the relative expression level of target genes according to the expression level of *TUB2*.

cDNA samples were synthesized from RNA extracted from *mips1*, *mips2*, *mips3*, and wild-type *Arabidopsis* rosette leaves using the methods described above. Gene-specific primers for the *MIPS* gene and the *TUB2* gene (see Supplemental Table 1 online) were used for RT-PCR.

Plant Materials and Growth Conditions

The *mips1* (SALK_023626) and *mips2* (SALK_031689) *Arabidopsis* mutants were obtained from the ABRC, and the left borders of insertion T-DNA were confirmed by sequencing of amplified PCR products. The *MIPS3* knockout mutant (*mips3*) with PPT resistance was identified from a pool of *Arabidopsis* (Columbia ecotype) T-DNA insertion lines (Qin et al., 2005), and the insertion site was detected by thermal asymmetric interlaced PCR and confirmed by DNA sequencing of the T-DNA inserts, segregation analysis, and RT-PCR. All the other T-DNA insertion lines used in this study were requested from the ABRC, and the homozygous lines and the T-DNA insertion sites were confirmed by PCR and sequencing. After sterilization and plating on solid half-strength Murashige and Skoog medium, seeds were stratified for 3 d at 4°C and then transferred to a continuously lit growth chamber at 22°C for germination. The seedlings were transplanted into potting soil 10 d later and were grown under long-day conditions (16 h light/8 h dark) with a light intensity of 120 µmol m^{-2} s^{-1} at 22°C and 60% relative humidity, unless stated otherwise. Double and triple mutants were obtained by crosses between the three single mutants mentioned above, and genotypes were determined by PCR (for primers, see Supplemental Table 1 online). For cotyledon phenotype analysis, we used seedlings at 8 DAG that had been grown under continuous light conditions. *pPIN1:PIN1-GFP* and *pDR5rev:GFP* lines (Friml et al., 2003) were crossed with the *mips1*$^{+/-}$ *mips2 mips3* mutant.

Phylogenetic Analysis

A total of 101 full-length amino acid sequences of MIPS proteins from eukaryotes (see Supplemental Data Set 1 online) were obtained from the National Center for Biotechnology Information by databank searching using the BLAST program (Altschul et al., 1990). Sequence alignment was performed using the ClustalW program (Thompson et al., 1994). The resultant PHYLIP file (see Supplemental Data Set 1 online) was analyzed by phylogenetic software PHYLIP 3.68 (Felsenstein, 2005). Yeast INO1 sequence was used as the outgroup for making rooted phylogenetic tree. A total of 1000 bootstrapped sequence sets were produced using SEQBOOT, and the tree file was processed by PROTPARS and CONSENSE programs. Visualization of the tree was performed using TreeView program (http://taxonomy.zoology.gla.ac.uk/rod/treeview.html).

Scanning Electron Microscopy

Cotyledons from 8-DAG *mips1 mips2*$^{+/-}$, *mips1 mips3*, and wild-type seedlings were collected and fixed in FAA (50% ethanol, 6% glacial acetic acid, and 5% formaldehyde) for 4 h at 25°C, followed by serial ethanol dehydration and isoamyl acetate substitution. Cotyledons were critical-point dried in liquid CO_2 and examined under a scanning electron microscope (Hitachi 4700) as described previously (Zhang et al., 2007).

Flow Cytometry

Cotyledons (1 to ~2 cm^2 each line) of 8-DAG *mips1 mips3* and wild-type seedlings that had been grown on solid half-strength Murashige and Skoog

medium were chopped in 50 μL chopping buffer (Galbraith et al., 1983) for 30 s, and then the suspension was filtered through a 50-μm nylon mesh and completed to a final volume of 500 mL with chopping buffer. The mixture was incubated with 10 μL 10 μg/mL RNase at 37°C for 20 min before addition of 2 μL 5 mg/mL propidium iodide and incubation in the dark for 20 min at 4°C. The resuspended nuclei were analyzed using a FACSCalibur flow cytometer (Becton Dickinson) with laser excitation at 488 nm. The DNA contents of nuclei were calculated by Cellquest (Becton Dickinson).

Whole-Mount Clearing and Fluorescence Detection of Embryos

For whole-mount preparations, embryos at different stages were mounted in a chloral hydrate/glycerol/water (8:1:3) mixture and cleared for 5 to 30 min, according to specific embryo developmental stage, before microscopy analysis. The mutant embryos containing *pPIN1:PIN1-GFP* or *pDR5rev:GFP* were dissected from seeds at specific developmental stages and mounted in a 6% glucose solution. Observation of GFP signals was performed using a Leica TCS SPE confocal with DM4000B microscope (Leica). The excitation wavelength of samples was 488 nm and emission was detected between 520 and 580 nm. For AM1-43 staining, *Arabidopsis* embryos at a specific stage were carefully dissected from developing seeds and incubated on ice with 5 μM of AM1-43 (Biotium) prepared in a 6% glucose solution, washed with 6% glucose solution, and mounted in the same solution for visualization. Embryos were then analyzed under a Leica TCS SPE confocal microscope.

Gas Chromatography Analysis

Three biological replications were performed for each genotype. For each experiment, 20 mg seeds were frozen and ground in liquid nitrogen, and 1 mL 80% methanol was added with 100 mM of ribitol as an internal standard. The mixture was incubated in 60°C for 1 h and centrifuged at 10,000g and 4°C for 15 min. The soluble part was removed to a new tube, centrifuged again, and dried at 45°C under a clean nitrogen stream. Freshly prepared derivatization reagent [250 μL; 1:1 mixture of pyridine and *N,O*-bis(trimethylsilyl)trifluoroacetamide + 1% trimethylchlorosilane] was added to each sample and vortexed for 20 min, and the mixture was incubated in 80°C for 15 min. Each sample was added with 250 μL hexane before injection. Gas chromatography–mass spectrometry analysis was performed by Agilent 6890 GC/5975B MSD (Agilent Technologies). Samples were loading to an autosampler and injected with a split of 4.8 mL min^{-1}. Separation was performed by helium gas stream with a controlled flow pressure of 8.81 p.s.i. and a linear velocity of 1 mL min^{-1}. The injection port was set as described (Torabinejad et al., 2009). The mass spectrometer was equipped with a DB-225MS capillary column (30 m × 0.25 mm i.d.; J&W Scientific). Quantification of *myo*-inositol was calculated by the standard curve of *myo*-inositol and the recovery of internal standard ribitol. All the chemicals used in this experiment were purchased from Sigma-Aldrich.

Histochemical Staining

Supplemental Table 1 online shows primers used in vector construction for GUS assays. Promoters for *MIPS1*, *MIPS2*, and *MIPS3* were amplified from *Arabidopsis* genomic DNA and cloned into vector pCAMBIA1391Xa (CAMBIA), pCAMBIA1391Xb (CAMBIA), and the gateway vector pBGWFS7 (VIB-Ghent University), respectively. Siliques were dissected from both sides and fixed in 80% acetone for 20 min. Samples were washed with 0.1 M sodium phosphate buffer, pH 7.0, and immersed in GUS staining solution (0.5 mg/mL 5-bromo-4-chloro-3-indolyl glucuronide, 10 mM Na$_2$EDTA, 0.5 mM potassium ferricyanide/ferrocyanide, and 0.06% Triton X-100 in 0.1 M Na$_2$HPO$_4$, pH 7.0) (Guo et al., 2009). The staining solution was vacuum infiltrated into samples for 10 min, and

samples were then incubated at 37°C for 4 h. Siliques were cleared in 70% ethanol before microscopy. Trypan blue staining of the wild type and *mips* double mutants was performed as described by Koch and Slusarenko (1990).

Transmission Electron Microscopy

Developing seeds at specific stages were collected and fixed in 2% glutaraldehyde and 2% formaldehyde in 0.1 M sodium phosphate buffer, pH 6.8, for 3 h at room temperature and then for 24 h at 4°C. Seeds were then washed three times with 0.1 M sodium phosphate buffer and postfixed in 1% O$_S$O$_4$ for 1 h, followed by dehydration in a graded acetone series. Seeds were embedded in a complete resin mixture (Spi-chem Spurr) and incubated in 70°C for 9 h. Samples were sectioned using a Leica EM UC6 ultramicrotome and stained with uranyl acetate and lead stain solutions. Sections were examined with a JEOL electron microscope.

HPLC-MS Analysis

The synthesis of IAA-*myo*-inositol was performed by reaction of imidazolated IAA and sodium *myo*-inositolate in DMSO as decribed before (Nowaki et al., 1978). The reaction mixture was stored at −20°C until use. The synthesized IAA-*myo*-inositol was diluted 1000-fold using 1% aqueous formic acid before HPLC-MS sample loading.

Roots of *Arabidopsis* germinating seeds were dissected and pooled. For a single experiment, 10 mg roots were grounded in liquid nitrogen and extracted with 500 μL prechilled methanol for 1 h (120 rpm, 4°C). After centrifugation, the residue was reextracted for 20 min. The supernatant was combined and passed through a 0.45-μm filter. The filtrate was evaporated in vacuo and resolved in 15 μL 1% aqueous formic acid. For *Arabidopsis* siliques and maize (*Zea mays*) kernels, 50 mg tissues were grounded in liquid nitrogen and treated following the same procedure described above. One injection of 10 μL was analyzed by Agilent HPLC 1200 coupled with a ZORBAX Eclipse Plus C18 column (150 mm × 2.1 mm; 5 μm; Agilent) that was used for the separation. The column thermostat was set at 30°C. The mobile phase was consisted of A, methanol, and B, 0.02% aqueous formic acid, at flow rate of 0.25 mL/min. The initial mobile phase was 20% A and 80% B. A linear gradient to 30% A and 70% B in 10 min was performed. The MS conditions were as follows: gas temperature, 350°C; gas flow, 12 L/min; nebulizer, 35 p.s.i.; capillary voltage, 2000 V; fragmentor, 125 V. The IAA-*myo*-inositol contents were calculated by the peak area of extracted ion current of $[M+H]^+$(338.123). Every isomer of IAA-*myo*-inositol from roots extract was confirmed by comparing MS^2 spectra with those of synthesized IAA-*myo*-inositol.

Accession Numbers

Sequence data can be found in the GenBank/EMBL database under the following accession numbers: *MPS1* (NM_120143; At4g39800), *MIPS2* (NM_127790; At2g22240), *MIPS3* (NM_121055; At5g10170), *PIS1* (NM_105470; At1g68000), *PIS2* (NM_120018; At4g38570), and *UGT84B1* (NM_127890; At2g23260), respectively. Accession numbers used for the phylogenetic analysis in Supplemental Figure 1 online can be found in Supplemental Table 2 online. T-DNA insertion lines used for mutant analysis were as follows: *mips1* (SALK_023626), *mips2* (SALK_031685), and *mips3* (N.070710 from the T-DNA insertion mutant collection generated in our laboratory). Other T-DNA insertion lines that were used for phenotype confirmation (Figure 4A) were SALK_023813, CS851587, SALK_108779C, SALK_120131, and SALK_068584.

Supplemental Data

The following materials are available in the online version of this article.

Supplemental Figure 1. Phylogenetic Tree of Eukaryotic MIPS Proteins.

Supplemental Figure 2. Expression Patterns of the Three *MIPS* Genes in Different *Arabidopsis* Tissues.

Supplemental Figure 3. Phenotypes of *mips* Double and Triple Mutants and Their Trypan Blue Staining Assays.

Supplemental Figure 4. PIN1 Localization in Globular Stage Embryos of Wild-Type and *mips1 mips3* Double Mutant upon BFA Treatment.

Supplemental Figure 5. Numbers of Trafficking Vesicles in Wild-Type, *mips1 mips3* Double Mutant, and PIS2-OX Embryo Cells.

Supplemental Table 1. Primers Used in This Study.

Supplemental Table 2. Accession Numbers for the Sequences Used in the Alignment in Supplemental Figure 1 and Supplemental Data Set 1.

Supplemental Data Set 1. Text File of the Sequences and Alignment Used for the Phylogenetic Analysis Shown in Supplemental Figure 1.

REFERENCES

Abreu, E.F.M., and Aragão, F.J.L. (2007). Isolation and characterization of a *myo*-inositol-1-phosphate synthase gene from yellow passion fruit (*Passiflora edulis f. flavicarpa*) expressed during seed development and environmental stress. Ann. Bot. (Lond.) **99:** 285–292.

Aida, M., Ishida, T., Fukaki, H., Fujisawa, H., and Tasaka, M. (1997). Genes involved in organ separation in *Arabidopsis*: An analysis of the cup-shaped cotyledon mutant. Plant Cell **9:** 841–857.

Alberti, S., Gitler, A.D., and Lindquist, S. (2007). A suite of Gateway cloning vectors for high-throughput genetic analysis in *Saccharomyces cerevisiae.* Yeast **24:** 913–919.

Altschul, S.F., Gish, W., Miller, W., Myers, E.W., and Lipman, D.J. (1990). Basic local alignment search tool. J. Mol. Biol. **215:** 403–410.

Bachhawat, N., and Mande, S.C. (2000). Complex evolution of the inositol-1-phosphate synthase gene among archaea and eubacteria. Trends Genet. **16:** 111–113.

Bennet, S.R.M., Alvarez, J., Bossinger, G., and Smyth, D. (1995). Morphogenesis in pinoid mutants of *Arabidopsis thaliana.* Plant J. **8:** 505–520.

Berleth, T., and Jürgens, G. (1993). The role of the monopteros gene in organising the basal body region of the *Arabidopsis* embryo. Development **118:** 575–587.

Bolte, S., Talbot, C., Boutte, Y., Catrice, O., Read, N.D., and Satiat-

Jeunemaitre, B. (2004). FM-dyes as experimental probes for dissecting vesicle trafficking in living plant cells. J. Microsc. **214:** 159–173.

Borner, G.H.H., Sherrier, D.J., Weimar, T., Michaelson, L.V., Hawkins, N.D., Macaskill, A., Napier, J.A., Beale, M.H., Lilley, K.S., and Dupree, P. (2005). Analysis of detergent-resistant membranes in *Arabidopsis*. Evidence for plasma membrane lipid rafts. Plant Physiol. **137:** 104–116.

Brinch-Pedersen, H., Sørensen, L.D., and Holm, P.B. (2002). Engineering crop plants: Getting a handle on phosphate. Trends Plant Sci. **7:** 118–125.

Buccafusca, R., Venditti, C.P., Kenyon, L.C., Johanson, R.A., Van Bockstaele, E., Ren, J., Pagliardini, S., Minarcik, J., Golden, J.A., Coady, M.J., Greer, J.J., and Berry, G.T. (2008). Characterization of the null murine sodium/*myo*-inositol cotransporter 1 (Smit1 or Slc5a3) phenotype: *myo*-inositol rescue is independent of expression of its cognate mitochondrial ribosomal protein subunit 6 (*Mrps6*) gene and of phosphatidylinositol levels in neonatal brain. Mol. Genet. Metab. **95:** 81–95.

Cantley, L.C. (2002). The phosphoinositide 3-kinase pathway. Science **296:** 1655–1657.

Chandler, J.W. (2008). Cotyledon organogenesis. J. Exp. Bot. **59:** 2917–2931.

Chaouch, S., and Noctor, G. (2010). *Myo*-inositol abolishes salicylic acid-dependent cell death and pathogen defence responses triggered by peroxisomal hydrogen peroxide. New Phytol. **188:** 711–718.

Chen, H., and Xiong, L. (2010). *myo*-Inositol-1-phosphate synthase is required for polar auxin transport and organ development. J. Biol. Chem. **285:** 24238–24247.

Chiu, T.T.Y., Rogers, M.S., Briton-Jones, C., and Haines, C. (2003). Effects of *myo*-inositol on the in-vitro maturation and subsequent development of mouse oocytes. Hum. Reprod. **18:** 408–416.

Collin, S., Justin, A.-M., Cantrel, C., Arondel, V., and Kader, J.-C. (1999). Identification of AtPIS, a phosphatidylinositol synthase from *Arabidopsis.* Eur. J. Biochem. **262:** 652–658.

Culbertson, M.R., Donahue, T.F., and Henry, S.A. (1976). Control of inositol biosynthesis in *Saccharomyces cerevisiae*: Properties of a repressible enzyme system in extracts of wild-type (Ino+) cells. J. Bacteriol. **126:** 232–242.

Cullen, P.J., Cozier, G.E., Banting, G., and Mellor, H. (2001). Modular phosphoinositide-binding domains–Their role in signalling and membrane trafficking. Curr. Biol. **11:** 882–893.

Donahue, J.L., Alford, S.R., Torabinejad, J., Kerwin, R.E., Nourbakhsh, A., Ray, W.K., Hernick, M., Huang, X., Lyons, B.M., Hein, P.P., and Gillaspy, G.E. (2010). The *Arabidopsis thaliana Myo*-inositol 1-phosphate synthase1 gene is required for *Myo*-inositol synthesis and suppression of cell death. Plant Cell **22:** 888–903.

Donahue, T.F., and Henry, S.A. (1981). *myo*-Inositol-1-phosphate synthase. Characteristics of the enzyme and identification of its structural gene in yeast. J. Biol. Chem. **256:** 7077–7085.

Eagle, H., Oyama, V.I., Levy, M., and Freeman, A.E. (1957). *Myo*-Inositol as an essential growth factor for normal and malignant human cells in tissue culture. J. Biol. Chem. **226:** 191–205.

Felsenstein, J. (2005). PHYLIP (Phylogeny Inference Package) Version 3.6. (Seattle, WA: University of Washington).

Fisher, S.K., Novak, J.E., and Agranoff, B.W. (2002). Inositol and higher inositol phosphates in neural tissues: Homeostasis, metabolism and functional significance. J. Neurochem. **82:** 736–754.

Friml, J., Vieten, A., Sauer, M., Weijers, D., Schwarz, H., Hamann, T., Offringa, R., and Jürgens, G. (2003). Efflux-dependent auxin gradients establish the apical-basal axis of *Arabidopsis.* Nature **426:** 147–153.

Galbraith, D.W., Harkins, K.R., Maddox, J.M., Ayres, N.M., Sharma,

D.P., and Firoozabady, E. (1983). Rapid flow cytometric analysis of the cell cycle in intact plant tissues. Science **220:** 1049–1051.

Ghosh Dastidar, K., Maitra, S., Goswami, L., Roy, D., Das, K.P., and Majumder, A.L. (2006). An insight into the molecular basis of salt tolerance of L-*myo*-inositol 1-P synthase (PcINO1) from *Porteresia coarctata* (Roxb.) Tateoka, a halophytic wild rice. Plant Physiol. **140:** 1279–1296.

Greene, N.D.E., and Copp, A.J. (1997). Inositol prevents folate-resistant neural tube defects in the mouse. Nat. Med. **3:** 60–66.

Guo, Y., Qin, G., Gu, H., and Qu, L.-J. (2009). Dof5.6/HCA2, a Dof transcription factor gene, regulates interfascicular cambium formation and vascular tissue development in Arabidopsis. Plant Cell **21:** 3518–3534.

Hall, P.J., and Bandurski, R.S. (1986). [³H]Indole-3-acetyl-*myo*-inositol hydrolysis by extracts of *Zea mays* L. vegetative tissue. Plant Physiol. **80:** 374–377.

Hanley, M.R., Jackson, T.R., Vallejo, M., Patterson, S.I., Thastrup, O., Lightman, S., Rogers, J., Henderson, G., and Pini, A. (1988). Neural function: Metabolism and actions of inositol metabolites in mammalian brain. Philos. Trans. R. Soc. Lond. B Biol. Sci. **320:** 381–398.

Harwood, J.L. (1980). Plant acyl lipids: Structure, distribution and analysis. In The Biochemistry of Plants, P.K. Stumpf, ed (New York: Academic Press), pp. 1–55.

Hegeman, C.E., Good, L.L., and Grabau, E.A. (2001). Expression of D-myo-inositol-3-phosphate synthase in soybean. Implications for phytic acid biosynthesis. Plant Physiol. **125:** 1941–1948.

Hynes, A.C., Sreenan, J.M., and Kane, M.T. (2000). Uptake and incorporation of *myo*-inositol by bovine preimplantation embryos from two-cell to early blastocyst stages. Mol. Reprod. Dev. **55:** 265–269.

Irvine, R.F., and Schell, M.J. (2001). Back in the water: The return of the inositol phosphates. Nat. Rev. Mol. Cell Biol. **2:** 327–338.

Jackson, R.G., Lim, E.-K., Li, Y., Kowalczyk, M., Sandberg, G., Hoggett, J., Ashford, D.A., and Bowles, D.J. (2001). Identification and biochemical characterization of an *Arabidopsis* indole-3-acetic acid glucosyltransferase. J. Biol. Chem. **276:** 4350–4356.

Johnson, M.D., and Sussex, I.M. (1995). 1 L-*myo*-inositol 1-phosphate synthase from *Arabidopsis thaliana.* Plant Physiol. **107:** 613–619.

Johnson, M.D., and Wang, X. (1996). Differentially expressed forms of 1-L-*myo*-inositol-1-phosphate synthase (EC 5.5.1.4) in *Phaseolus vulgaris*. J. Biol. Chem. **271:** 17215–17218.

Kane, M.T., Norris, M., and Harrison, R.A.P. (1992). Uptake and incorporation of inositol by preimplantation mouse embryos. J. Reprod. Fertil. **96:** 617–625.

Kesy, J.M., and Bandurski, R.S. (1990). Partial purification and characterization of indol-3-ylacetylglucose:*myo*-inositol indol-3-ylacetyltransferase (indoleacetic acid-inositol synthase). Plant Physiol. **94:** 1598–1604.

Kleine-Vehn, J., and Friml, J. (2008). Polar targeting and endocytic recycling in auxin-dependent plant development. Annu. Rev. Cell Dev. Biol. **24:** 447–473.

Koch, E., and Slusarenko, A. (1990). *Arabidopsis* is susceptible to infection by a downy mildew fungus. Plant Cell **2:** 437–445.

Krauß, M., and Haucke, V. (2007). Phosphoinositide-metabolizing enzymes at the interface between membrane traffic and cell signalling. EMBO Rep. **8:** 241–246.

Liu, J., et al. (2008). Targeted degradation of the cyclin-dependent kinase inhibitor ICK4/KRP6 by RING-type E3 ligases is essential for mitotic cell cycle progression during *Arabidopsis* gametogenesis. Plant Cell **20:** 1538–1554.

Livak, K.J., and Schmittgen, T.D. (2001). Analysis of relative gene expression data using real-time quantitative PCR and the 2(-Delta Delta C(T)) Method. Methods **25:** 402–408.

Loewus, F.A., ed (1973). Biogenesis of Plant Cell Wall Polysaccharides. (New York: Academic Press).

Loewus, F.A., and Murthy, P.P.N. (2000). *myo*-Inositol metabolism in plants. Plant Sci. **150:** 1–19.

Löfke, C., Ischebeck, T., König, S., Freitag, S., and Heilmann, I. (2008). Alternative metabolic fates of phosphatidylinositol produced by phosphatidylinositol synthase isoforms in *Arabidopsis thaliana*. Biochem. J. **413:** 115–124.

Macbeth, M.R., Schubert, H.L., Vandemark, A.P., Lingam, A.T., Hill, C.P., and Bass, B.L. (2005). Inositol hexakisphosphate is bound in the ADAR2 core and required for RNA editing. Science **309:** 1534–1539.

Majumder, A.L., Chatterjee, A., Ghosh Dastidar, K., and Majee, M. (2003). Diversification and evolution of L-*myo*-inositol 1-phosphate synthase. FEBS Lett. **553:** 3–10.

Melaragno, J.E., Mehrotra, B., and Coleman, A.W. (1993). Relationship between endopolyploidy and cell size in epidermal tissue of *Arabidopsis.* Plant Cell **5:** 1661–1668.

Meng, P.H., Raynaud, C., Tcherkez, G., Blanchet, S., Massoud, K., Domenichini, S., Henry, Y., Soubigou-Taconnat, L., Lelarge-Trouverie, C., Saindrenan, P., Renou, J.P., and Bergounioux, C. (2009). Crosstalks between *myo*-inositol metabolism, programmed cell death and basal immunity in *Arabidopsis.* PLoS ONE **4:** e7364.

Michell, R.H. (2008). Inositol derivatives: Evolution and functions. Nat. Rev. Mol. Cell Biol. **9:** 151–161.

Miller, B.L., Moats, R.A., Shonk, T., Ernst, T., Woolley, S., and Ross, B.D. (1993). Alzheimer disease: Depiction of increased cerebral myo-inositol with proton MR spectroscopy. Radiology **187:** 433–437.

Mitsuhashi, N., Kondo, M., Nakaune, S., Ohnishi, M., Hayashi, M., Hara-Nishimura, I., Richardson, A., Fukaki, H., Nishimura, M., and Mimura, T. (2008). Localization of *myo*-inositol-1-phosphate synthase to the endosperm in developing seeds of *Arabidopsis.* J. Exp. Bot. **59:** 3069–3076.

Murphy, A.M., Otto, B., Brearley, C.A., Carr, J.P., and Hanke, D.E. (2008). A role for inositol hexakisphosphate in the maintenance of basal resistance to plant pathogens. Plant J. **56:** 638–652.

Nawy, T., Lukowitz, W., and Bayer, M. (2008). Talk global, act local-patterning the *Arabidopsis* embryo. Curr. Opin. Plant Biol. **11:** 28–33.

Nelson, D.E., Rammesmayer, G., and Bohnert, H.J. (1998). Regulation of cell-specific inositol metabolism and transport in plant salinity tolerance. Plant Cell **10:** 753–764.

Normanly, J. (2010). Approaching cellular and molecular resolution of auxin biosynthesis and metabolism. Cold Spring Harb. Perspect. Biol. **2:** a001594.

Nowaki, J., Cohen, J.D., and Bandurski, R.S. (1978). Synthesis of ¹⁴C-indole-3-acetic-*myo*-inositol. J. Labelled Compd. Rad. **15:** 325–329.

Nunez, L.R., Jesch, S.A., Gaspar, M.L., Almaguer, C., Villa-Garcia, M., Ruiz-Noriega, M., Patton-Vogt, J., and Henry, S.A. (2008). Cell wall integrity MAPK pathway is essential for lipid homeostasis. J. Biol. Chem. **283:** 34204–34217.

Papaleo, E., Unfer, V., Baillargeon, J.P., and Chiu, T.T. (2009). Contribution of *myo*-inositol to reproduction. Eur. J. Obstet. Gynecol. Reprod. Biol. **147:** 120–123.

Peskan, T., Westermann, M., and Oelmüller, R. (2000). Identification of low-density Triton X-100-insoluble plasma membrane microdomains in higher plants. Eur. J. Biochem. **267:** 6989–6995.

Qin, G., Gu, H., Zhao, Y., Ma, Z., Shi, G., Yang, Y., Pichersky, E., Chen, H., Liu, M., Chen, Z., and Qu, L.-J. (2005). An indole-3-acetic acid carboxyl methyltransferase regulates *Arabidopsis* leaf development. Plant Cell **17:** 2693–2704.

Sarkar, S., Floto, R.A., Berger, Z., Imarisio, S., Cordenier, A., Pasco, M., Cook, L.J., and Rubinsztein, D.C. (2005). Lithium induces

autophagy by inhibiting inositol monophosphatase. J. Cell Biol. **170:** 1101–1111.

Schapire, A.L., Voigt, B., Jasik, J., Rosado, A., Lopez-Cobollo, R., Menzel, D., Salinas, J., Mancuso, S., Valpuesta, V., Baluska, F., and Botella, M.A. (2008). *Arabidopsis* synaptotagmin 1 is required for the maintenance of plasma membrane integrity and cell viability. Plant Cell **20:** 3374–3388.

Shaltiel, G., Shamir, A., Shapiro, J., Ding, D., Dalton, E., Bialer, M., Harwood, A.J., Belmaker, R.H., Greenberg, M.L., and Agam, G. (2004). Valproate decreases inositol biosynthesis. Biol. Psychiatry **56:** 868–874.

Simonsen, A., Wurmser, A.E., Emr, S.D., and Stenmark, H. (2001). The role of phosphoinositides in membrane transport. Curr. Opin. Cell Biol. **13:** 485–492.

Stevenson-Paulik, J., Bastidas, R.J., Chiou, S.T., Frye, R.A., and York, J.D. (2005). Generation of phytate-free seeds in *Arabidopsis* through disruption of inositol polyphosphate kinases. Proc. Natl. Acad. Sci. USA **102:** 12612–12617.

Tan, X., Calderon-Villalobos, L.I.A., Sharon, M., Zheng, C., Robinson, C.V., Estelle, M., and Zheng, N. (2007). Mechanism of auxin perception by the TIR1 ubiquitin ligase. Nature **446:** 640–645.

Tanaka, H., Dhonukshe, P., Brewer, P.B., and Friml, J. (2006). Spatiotemporal asymmetric auxin distribution: A means to coordinate plant development. Cell. Mol. Life Sci. **63:** 2738–2754.

Thole, J.M., and Nielsen, E. (2008). Phosphoinositides in plants: Novel functions in membrane trafficking. Curr. Opin. Plant Biol. **11:** 620–631.

Thompson, J.D., Higgins, D.G., and Gibson, T.J. (1994). CLUSTAL W: Improving the sensitivity of progressive multiple sequence alignment through sequence weighting, position-specific gap penalties and weight matrix choice. Nucleic Acids Res. **22:** 4673–4680.

Tiede, A., Bastisch, I., Schubert, J., Orlean, P., and Schmidt, R.E. (1999). Biosynthesis of glycosylphosphatidylinositols in mammals and unicellular microbes. Biol. Chem. **380:** 503–523.

Torabinejad, J., Donahue, J.L., Gunesekera, B.N., Allen-Daniels, M.J., and Gillaspy, G.E. (2009). VTC4 is a bifunctional enzyme that affects myoinositol and ascorbate biosynthesis in plants. Plant Physiol. **150:** 951–961.

Ueda, T., Yamaguchi, M., Uchimiya, H., and Nakano, A. (2001). Ara6, a plant-unique novel type Rab GTPase, functions in the endocytic pathway of *Arabidopsis thaliana.* EMBO J. **20:** 4730–4741.

Wheeler, G.L., and Brownlee, C. (2008). Ca^{2+} signalling in plants and green algae—Changing channels. Trends Plant Sci. **13:** 506–514.

Winkel-Shirley, B. (2002). Biosynthesis of flavonoids and effects of stress. Curr. Opin. Plant Biol. **5:** 218–223.

Xue, H.-W., Hosaka, K., Plesch, G., and Mueller-Roeber, B. (2000). Cloning of *Arabidopsis thaliana* phosphatidylinositol synthase and functional expression in the yeast *pis* mutant. Plant Mol. Biol. **42:** 757–764.

Yoshida, K.T., Wada, T., Koyama, H., Mizobuchi-Fukuoka, R., and Naito, S. (1999). Temporal and spatial patterns of accumulation of the transcript of *Myo*-inositol-1-phosphate synthase and phytin-containing particles during seed development in rice. Plant Physiol. **119:** 65–72.

Zhang, X., Chen, Y., Wang, Z.-Y., Chen, Z., Gu, H., and Qu, L.-J. (2007). Constitutive expression of CIR1 (RVE2) affects several circadian-regulated processes and seed germination in *Arabidopsis.* Plant J. **51:** 512–525.

Zimmermann, P., Hirsch-Hoffmann, M., Hennig, L., and Gruissem, W. (2004). GENEVESTIGATOR. *Arabidopsis* microarray database and analysis toolbox. Plant Physiol. **136:** 2621–2632.